ISSN 1075-7015, Geology of Ore Deposits, 2021, Vol. 63, No. 1, pp. 1–33. © Pleiades Publishing, Ltd., 2021.
Russian Text © The Author(s), 2021, published in Geologiya Rudnykh Mestorozhdenii, 2021, Vol. 63, No. 1, pp. 3–39.

Forms of Gold and Some Typomorphic Characteristics of Native Gold of the Pavlik Orogenic Deposit (Magadan Oblast)

V. V. Aristov[a, b, *], A. V. Grigorieva[a], Yu. S. Savchuk[a], N. V. Sidorova[a], and V. A. Sidorov[c]

[a] *Institute of Geology of Ore Deposits, Petrography, Mineralogy and Geochemistry, Russian Academy of Sciences, Moscow, Russia*

[b] *Institute of Geology of Diamond and Precious Metals, Siberian Branch, Russian Academy of Sciences, Yakutsk, Russia*

[c] *OJSC Pavlik Gold Company, Magadan, Russia*

**e-mail: rstvvv@yandex.ru*

Received July 17, 2018; revised June 9, 2020; accepted June 15, 2020

Abstract—The ratios of vein and ore minerals bearing native gold, the shape and size native gold particles, their surface features, variations in chemical composition, and the presence and distribution of impurities and inclusions in them, allow sufficiently substantiated assumptions about ore-forming settings and composition, phase state, and certain other parameters of ore-forming fluids that precipitated native gold. If these data are insufficient for a full-fledged judgment on the ore formation processes, they can at least be used to curtail various genetic speculations. Certain typomorphic features of native gold were studied from one of the largest orogenic gold deposits in northeastern Russia. New data on the grain size distriubtion and chemical composition of native gold and gold contents in sulfides of the Pavlik deposit were obtained. Optical and SEM images were used to determine the ore texture, morphology, and internal structure of native gold and auriferous pyrite and arsenopyrite. ICP-MS, EDS, EDX were used to assess the composition of gold grains, EPMA and LA-ICP-MS were used to qualitatively and quantitatively characterize gold-bearing grains of pyrite and arsenopyrite. It was established that microscopic (finely dispersed (>0.0005–0.01), dusty (>0.01–0.05), extremely fine (>0.05–0.1)) (peak size at 0.075 mm), visible (very fine (>0.1 –0.25)), and fine (>0.25–1.00)) (size peaks at 0.25, 0.55 and 0.85 mm) native gold in association with sphalerite, pyrrhotite, pyrite, arsenopyrite, quartz, carbonates, albite, and sericite is widespread at the Pavlik deposit. Gold particles with an average size of 0.3 mm predominate by weight. Comparison of grain size distribution data with the technological properties of ores and the results of mining in the Omchak ore–placer district made it possible to establish that the share of dusty and fine-dispersed size classes accounts for at least 15–20% of the gold mass at the deposit.

ICP-MS analysis of a bulk sample of a monofraction of native gold, which included native gold grains from different parts of the deposit, showed that the composition of the monofraction includes Fe, Hg, As, Zn, Cu, and Pb impurities. The average gold fineness was 806 with additional peaks of 775, 855, and 985 (EPMA determinations). The heterogeneity of native gold is due to the redistribution of silver during late deformation events and, to a lesser extent, removal of silver from gold in the ore oxidation zone. Inclusions in gold are represented by microvoids, disseminated fragments of host metasomatites, and crystals or crystal fragments of potassium feldspar, albite, ankerite–dolomite, and arsenopyrite. The low gold content in pyrite and arsenopyrite, with a high (up to 287 g/t) gold content in arsenic-bearing pyrite and ratios of molar amounts of gold and arsenic in arsenopyrite, may indicate that gold is bound in the crystal structure of sulfides. The relationship between native gold and vein and ore minerals, the features of native gold, and the regularities of gold distribution in pyrite and arsenopyrite do not contradict the hypothesis that native gold was deposited at a single mineralization stage in a different substrate: (1) in the intergranular space (quartz–carbonate metasomatites), (2) in the interstitial space (in arsenopyrite and carbonates), (3) in microfissures in the host minerals. Obviously, the deposition of native gold is an independent process occurring against a background of metamorphogenic (quartz–carbonate veins) and magmatic–metamorphogenic (disseminated pyrite and arsenopyrite) mineralization. Comparison of native gold from ore and placer objects of the Omchak ore–placer district has culminated in methods for using the typomorphic features of native gold to search for placer sources. It seems that various inclusions in native gold with a porous surface are promising for identifying old sources and reconstructing its crystallization conditions.

Keywords: Russian Northeast, Omchak ore–placer district, Pavlik deposit, orogenic gold deposits, gold–quartz ore objects, native gold typomorphism, ore formation, gold deposit prospecting

DOI: 10.1134/S1075701521010025

INTRODUCTION

Orogenic Au deposits (mesothermal, vein) currently include the family of mineral deposits formed during tectonic events at convergent tectonic plate boundaries (Goldfarb et al., 2005). According to calculations (Phillips, 2013), these deposits and their accompanying placers (excluding Witwatersrand) are responsible for about 45% of global Au production. Orogenic deposits have formed throughout the Earth's geological history, and they are maximally concentrated within Late Archean cratons, Paleoproterozoic mobile belts, and Phanerozoic orogenic fold–thrust belts (Goldfarb et al., 2001). Various ore-hosting rocks metamorphosed under upper–middle crustal temperature and pressure conditions (200–650°C and 1–5 kbar) (Groves, 1993; Tomkins and Grundy, 2009; Bortnikov, 2006; Bortnikov et al., 1998, 2004, 2007). Orogenic deposits are formed in a compression setting within large strike-slip zones (Groves et al., 2003). Fluids move along cleavage zones that developed layer-by-layer (intraformational fractures) and along subvertical regional fracture structures during major seismic events and/or a sharp increase in hydrostatic pressure (Cox, 2005).

As shown in recent reviews on orogenic gold deposits (Goldfarb et al., 2005; Goldfarb and Groves, 2015), the long debate about the genesis of these deposits is far from over. The authors of the reviews attribute this to the fact that orogenic gold deposits form at crustal depths from 3 to 15 km, and large objects younger than 50 Ma have not reached the surface; therefore, fluid sources cannot be studied directly. Various processes within or near gold deposition areas make it difficult to reconstruct the original chemical composition of the ore fluid. Extended fluid flow paths yield ambiguous interpretations of the data obtained in fluid inclusion (FI) and isotope studies. In addition, the formation of orogenic gold deposits encompasses an extremely broad time interval, during which the main changes in Earth's thermal state, its tectonosphere, hydrosphere, and atmosphere took place.

Citing for comparison 30-year-old data (Kerrich, 1991) and (Nesbitt, 1991), Goldfarb and Groves (2015) demonstrated that over that time, it was possible to amass reliable arguments against the hypothesis of meteoric waters taking part in ore formation and the absence of a genetic relationship between gold mineralization and halos from the development of lamprophyric magmatism. The main geological–genetic ore deposit formation models consider fluid sources to be various magmas (magmatogenic–hydrothermal), volcanosedimentary sequences with their metamorphic (metamorphogenic model) or metagenetic (lateral-secretion model) dewatering, volcanic activity synchronous with sedimentary accumulation (hydrothermal sedimentary model), and, lastly, the hypothesis on mantle sources of some fluids (Goldfarb and Groves, 2015 and references therein). In recent years, the idea of predominant metamorphogenic fluids removed during dewatering of the sedimentary cover and basalts of a subducting oceanic plate has won out over other models. New evidence was recently obtained by Prokofiev et al. (2020). In a core from the Kola superdeep borehole, highly-gold-bearing fluid inclusions have been established at depths from 9 to 11 km in gold-bearing quartz veins that formed during Proterozoic regressive metamorphism of Archean two-mica schists and amphibolites. The fluid inclusions contain gold nanoparticles. The sources of the gold and fluid itself are obviously exogenic (e.g., oceanic crust subducted in the Proterozoic), which were dewatered under amphibolite facies conditions. A hypothesis on the participation of magmatogenic and metamorphogenic fluids in the formation of orogenic (mesothermal) deposits is currently being developed at IGEM RAS (Bortnikov, 2006; Bortnikov et al., 1998, 2004; Vikent'eva et al., 2017).

Deposits hosting gold–quartz and gold(arsenic)–sulfide ore assemblages can be found in Russian ore-formation classifications that compare certain geological conditions of deposits with the compositions of productive mineral assemblages closest to orogenic gold deposits in Phanerozoic orogenic fold–thrust belts (see, e.g., (Konstantinov et al., 2000; *Prostranstvennye* ..., 2002; Safonov, 2010). One of Russia's largest gold-ore provinces in which such deposits are widespread is the Yano-Kolyma gold-bearing province (YKGP), which tectonically corresponds to the eastern part of the Mesozoic Yano-Kolyma fold region (fold–thrust belt). For over 90 years, almost 4000 t of gold have been mined from ore and, mainly, placer deposits in this belt (according to (Mikhailov et al., 2007) with an additional average annual output of about 20 t). The majority of modern researchers, following the generalizing work of Soviet and American geologists (*Metallogenesis* ..., 2005), classify gold objects that are the sources of a majority of placers, as typical orogenic gold deposits in terrigenous complexes (Voroshin et al, 2014).

In addition to geotectonic position (the rear zone of the fold–thrust belt of a collisional orogen (Aristov, 2019)), the features of host rocks (terrigenous sequences with a distinctly subordinate role of volcanic and carbonate deposits (Konstantinovskii, 2009), distinct control of en echelon structures of regional strike-slip faults (Shakhtyrov, 1997), and inconsistent relationships with granitoids (Voroshin et al., 2014; Goryachev., 2014), gold ore objects in the YKGP are characterized by an assemblage of closely spaced or partially spatially overlapping:

—zones and areas of noncoeval carbonate–sericite–albite–quartz metasomatites, carbonate–quartz veinlets, and banded and massive quartz veins (quartz zone);

—zones and areas of sulfide (pyrite–arsenic pyrite–arsenopyrite) impregnation in host rocks,

some metasomatites, and individual quartz veins and veinlets (sulfide zone);

—zones of gold mineralization (from finely dispersed to large veinlets) in host rocks, veinlets and veins, and sulfide impregnations (gold zone).

The ratios of quartz (free silica) and sulfides at the YKGP deposits can vary quite strongly (from 99 : 1 to 1 : 1), but these objects are conventionally called gold–quartz (Skornyakov, 1949). Although a detailed mineral composition study made it possible (Gamyanin, 2001) to distinguish polymetallic (galena–sphalerite), sulfosalt (boulangerite-bournonite), and antimonite (berthierite–antimonite) ores, geochemically, the ores are virtually monometallic. An exception is As, which is consistently present in ores, but not always in geochemical association with Au.

Below, we use both names of ore objects: gold–quartz in cases of specific deposits of the YKGP, as described above; for comparison with gold objects of other Phanerozoic orogenic belts, the term orogenic gold deposits is used.

For the gold–quartz ore objects of the YKGP, there are two groups of hypotheses on their genesis: the first does not separate the fluid sources from which the mineral assemblages of the quartz, sulfide, and gold zones formed, and the second envisages an independent source of gold, associated to varying degrees with sources of other fluids. The first group includes:

—the orthomagmatic hypothesis relating these objects with dikes, small intrusions, batholiths, or granitoid magma chambers in general (see, e.g., references in (Voroshin et al., 2014);

—the metamorphogenic hypothesis (Firsov, 1985), which is closer to the lateral-secretion hypothesis (Boyle, 1979) than to modern hypotheses on metamorphogenic sources of ores at orogenic deposits supported by North American geologists.

The second group of hypotheses includes:

—A hypotheses emphasizing the importance of host sequences as an intermediate gold source for deposit formation (Buryak et al., 2002; Sidorov and Thomson, 2000; Konstantinov, 2009), in particular: (1) host sequences enriched with disperse gold transported from ancient sources and deposited at organic and other barriers (Politov et al., 2008); (2) host sequences enriched in syngenetic (Kryazhev, 2017), diagenetic (Large, 2007), or contact-metamorphic (Tyukova and Voroshin, 2007) sulfides. Various thermal and tectonic events (programmatic metamorphism or emplacement of batholith intrusions) are considered as subsequent events that redistributed gold, which caused breakdown of sulfides and gold migration in the form of nanoparticles or disulfide complexes in accordance with temperature and pressure gradients.

—Modifications to the magmatogenic hypothesis, which emphasize the importance of magma transport and concentration of ore material (see e.g. (Bortnikov, 2006; Goryachev, 1998; Goryachev et al., 2008)), suggest that the magmatogenic fluid dominates during ore deposition; i.e., sources of gold and sulfide sulfur are located in deep-seated granitoid massifs, and the presence of a certain amount of metamorphogenic fluid is explained by contact metamorphism of the host sequences. Precision studies of sulfides of productive mineral assemblages at the Nezhdaninskoe orogenic gold deposit (Chernyshev et al., 2011; Chugaev et al., 2010) made it possible to prove the presence in their composition of both "magmatic" lead and lead removed from terrigenous rocks.

—The gold-bearing fluid is separated during mantle degassing (Anikeev et al., 1966; Gelman, 1976; Novgorodova et al., 2004), and the remaining fluids participating in the formation of veins and veinlets and quartz impregnation of the sulfide zone form in situ during different thermal and tectonic events, e.g., when sedimentary sequences subside to the level of fluid and magma generation (Konstantinov, 2009).

As noted by (Goldfarb and Groves, 2015), the data obtained on orogenic gold deposits from the results of FI studies, variations in the composition of stable and radiogenic isotopes, and the trace element composition of ores are interpreted ambiguously due to the complex formation history of the analyzed material.

For gold–quartz objects of the YKGP, the reasons for this ambiguity may be:

—the recurring mass formation of compositionally identical carbonate–quartz veinlets and accompanying alterations in host rocks in the quartz zone, which makes it difficult or almost impossible to verify the occurrence of any directional changes in the composition of ore-forming fluids;

—variability of the morphological and physicochemical properties of pyrite and arsenopyrite of the sulfide zone, which (i.e., the properties) are not unambiguously related to the productivity of orebodies, especially since a genetic relationship between sulfides of the sulfide zone and native gold has not yet been established;

—owing to the difficulty in identifying metasomatic alterations and vein minerals directly related to the formation of a productive mineral assemblage, the ratio of native gold to ore and vein minerals is debatable and can be interpreted in different ways;

—ore minerals of variable composition, which are usually considered indicators of the physicochemical ore deposition conditions, are absent within the gold zone or are found in ores in insignificant amounts; variations in the composition of these minerals evidence the surprising homogeneity of the ore-forming environment.

A significant number of gold–quartz objects are confined to long-lived shear zones and are located in an active neotectonic zone; therefore, the formation of secondary inclusions in deformed and regenerated

quartz can continue, and in reactivated tectonic zones, halogens and various noble gases may ascend to the surface, which can also be used to reconstruct the formation conditions of gold–quartz objects.

The diversity of the hypotheses also indicates that the broad range of mineralogical and geochemical data used allows researchers to more or less reliably substantiate their viewpoints. For example, the entire dataset on fluid inclusions and stable isotopes is attributed to quartz zone formations. The isotopic composition of sulfur and, in most cases, lead has been determined for minerals of the sulfide zone. However, the timing of the formation of the three zones, as well as the quantitative ratio of mineral-forming and ore-forming fluids, remains an open question and, moreover, can significantly affect the adoption of a particular genetic and, accordingly, prospecting model.

Goldfarb and Groves (2015) believe that the problem of choosing between models involving the evolution of one fluid and models in which several fluids evolve is generally philosophical and depends on the personal preferences of the researchers. However, it seems to us that the problem is not philosophical, but rather consists in the choice of research object and strict limitations of the data used. Consequently, questions arise: Which typomorphic features of which vein and ore minerals and what FI, isotope, and other data can be used to determine the formation conditions of native gold and, accordingly, as prospecting features of gold–quartz objects without additional qualifications?

In our opinion, to answer this question, it is necessary to study native gold. As different researchers have shown (Petrovskaya, 1973; Amosov and Vasin, 1995; *Samorodnoe* ..., 2015), the ratio of native gold to host minerals, its shape, size of segregations, surface features, variations in chemical composition, and the presence of impurities and inclusions permit fairly well-substantiated judgments about the permeability parameters of the ore-hosting medium, the composition, phase state, and certain *PT* parameters of the ore-forming fluids that deposited the native gold. If this is insufficient for full-fledged judgments about the ore formation processes, such parameters can be used to limit the diversity of genetic speculations.

Geological studies have repeatedly proved the possibility of using native gold with certain typomorphic features to predict the geological and economic type and scale of ore objects, as well as as a direct feature in prospecting for the primary sources of placers. The importance of identifying and comparing typomorphic features of native gold at gold–quartz objects of the YKGP is particularly high due to the ubiquitous development of placer gold occurrences in Quaternary deposits with low contrast and poorly expressed zoning of geochemical halos associated with mineralization. The morphology, size, and fineness of placer gold in the YKGP has been quite well researched; several published studies have generalized the data obtained during placer mining of (Savva and Preis, 1990; Amuzinsky et al., 1992; Moskvitin et al., 1997). The presence of native gold remains the only reliable indicator of the outlook of prospecting sites for gold–quartz objects, and variations in the morphology and composition of native gold in placer halos or primary occurrences at a site provide one of the few opportunities to establish the mineralogical and geochemical zoning of the mineralization, as shown for the YKGP (see, e.g., (Skryabin, 2010)). All these data were obtained from bulk samples; modern analytical research methods were used sporadically. Inhomogeneities and inclusions in native gold are not well understood. Typomorphic features of native gold from primary deposits have hardly been studied comprehensively and systematically, with few exceptions (Pluteshko et al., 1988; Ostapenko et al., 2004; Litvinenko, 2009).

The aim of this article is to identify the main gold species, to determine some features of native gold at the Pavlik gold–quartz deposit typical of the YKGP, and to show the directions in which these features may be used, both in genetic constructions and solving practical problems.

BRIEF GEOLOGY OF THE PAVLIK DEPOSIT ORE FIELD

The Pavlik deposit is located in the Omchak ore district (Fig. 1, inset) of the Ten'ka gold ore metallogenic zone. The Degdekan, Rodionovskoe, and Natalka deposits are in the same zone (Eremin et al., 1994;

Fig. 1. Geological structure of Pavlik deposit ore field. (1) Quaternary alluvial deposits; (2–5) Permian system, upper section: (2–4) Neryuchinskaya sequence: (2) upper subsequence: clay shale, (3) middle subsequence: silty-argillaceous shale, clayey sandstone, diamictite, conglomerate, (4) lower subsequence: silty-argillaceous shale, sandstone, diamictite; (5) Atkan sequence, diamictite with clayey sandstone and conglomerate lenses; (6–7) intrusive formations: (6) Late Cretaceous subvolcanic bodies of explosive rhyolites with numerous fragments of siltstone, diorite, quartz veins (Vanin stock) (*a*), dikes (*b*); (7) Early Cretaceous stocks of diorites (*a*), diorite dikes (*b*), lamprophyre dikes (*c*); (8) faults: Ten'kinsky fault (*a*), normal faults (*b*), strike-slip faults (*c*), thrust faults (*d*), inferred under the cover of Quaternary deposits (*e*); (9) quartz vein zones; (10) zones with vein-disseminated ankerite–quartz and pyrite–arsenopyrite mineralization (ore zones): in plan view (*a*), on section (*b*); (11) bedding elements. Inset: tectonic diagram of eastern part of Verkhoyansk–Kolyma fold belt (after (Aristov, 2019) with simplifications). (1) Upper Jurassic-Cenozoic orogenic formations: volcanic and terrigenous (*a*), granitoid (*b*); (2) Verkhoyansk–Kolyma sedimentary basin; (3) North Asian craton (Siberian Platform) and Kolyma–Omolon superterrane; (4) Okhotsk terrane; (5) modern lithospheric plate boundary ((NA, North American, EU, Eurasian, after (*Tektonika*.., 2001); (6) largest fault systems: reliably established (*a*), inferred (*b*); (7) Omchak ore–placer cluster (TR); (8) gold–quartz deposits: Natalka and Pavlik (*a*); other (*b*).

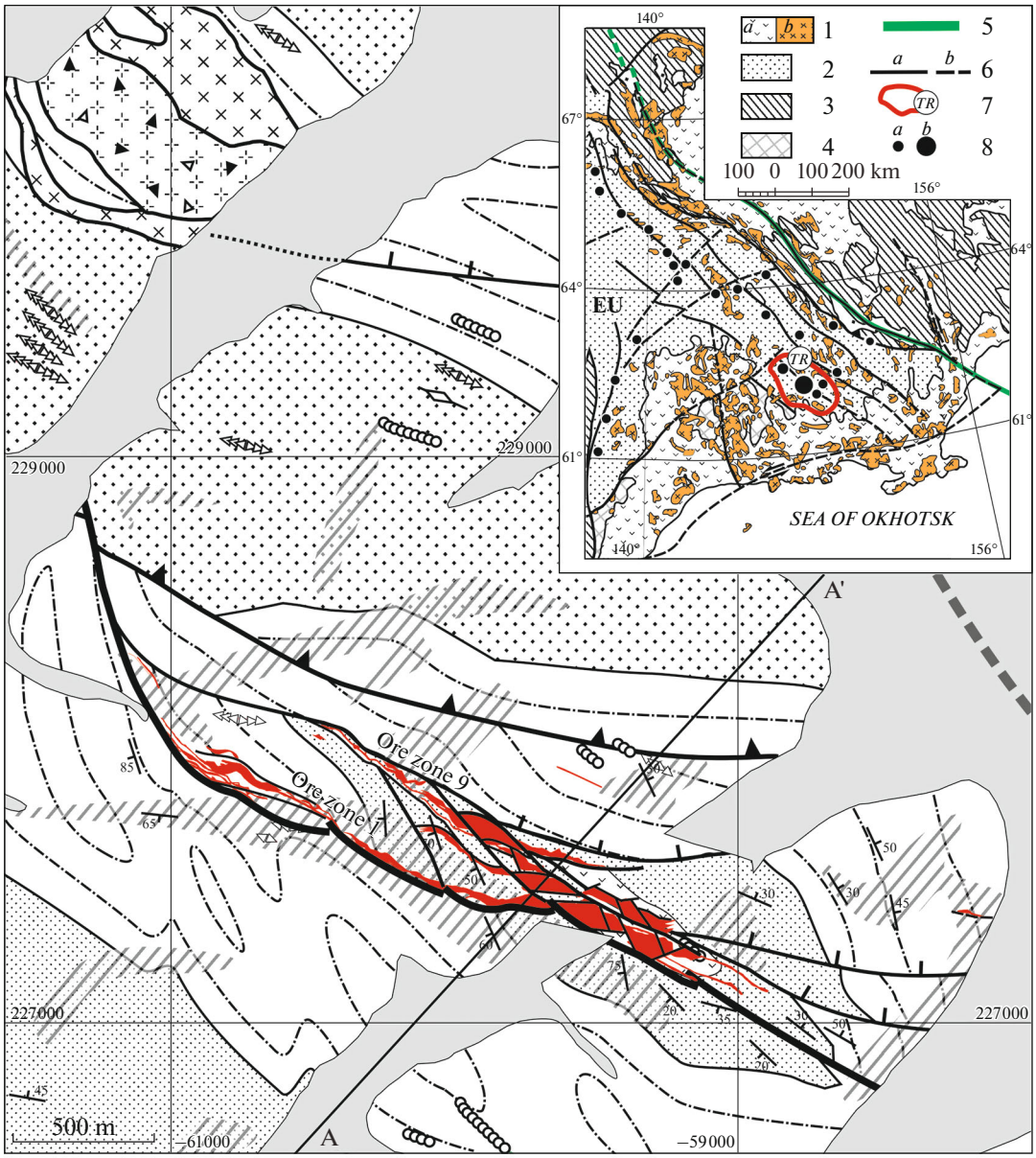

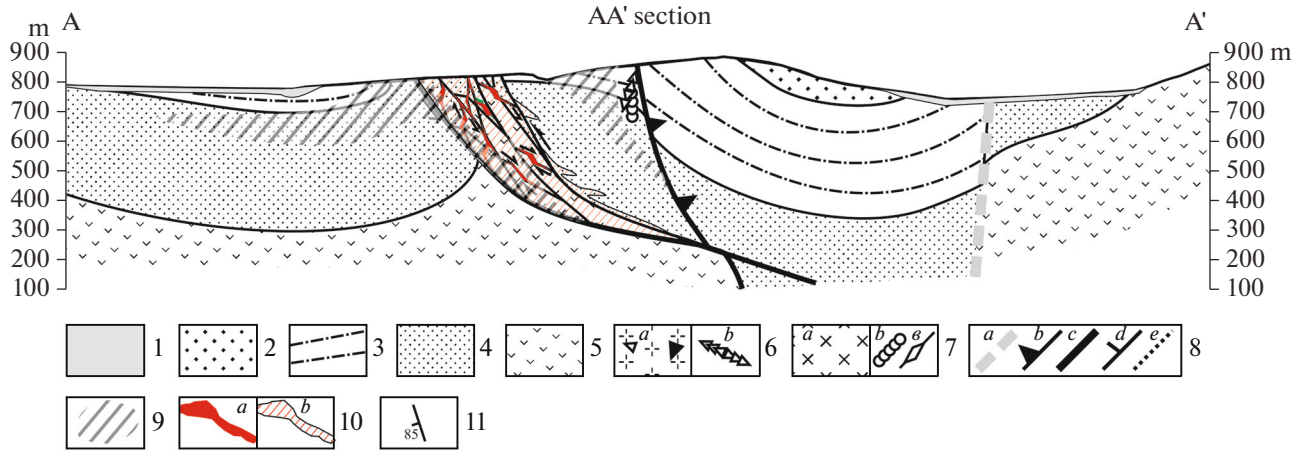

GEOLOGY OF ORE DEPOSITS Vol. 63 No. 1 2021

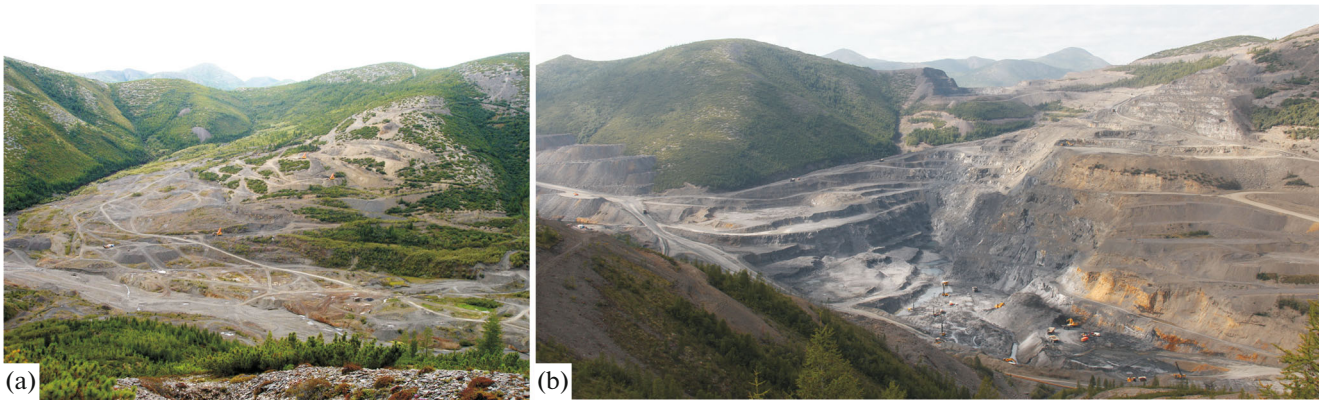

Fig. 2. Quarry of Pavlik deposit. Northwest view. (a) Before workings for 2008; (b) as of August 19, 2017.

Goncharov et al., 2002; Struzhkov et al., 2006; Goryachev et al., 2008). The Pavlik is one of the largest gold deposits in northern Russia. Gold resources of categories C1 + C2 (measured and indicated resources) for 2019 are about 220 t, and resources of category P1 (inferred resources) are at least 80 t (according to JSC Pavlik Gold Mining Company (https://www.arlan.ru/gold/activities/mineral-resources-base)).

The deposit was discovered by geologist N.A. Aseev almost simultaneously with the Natalka deposit (Goncharov et al., 2002), but for many years it remained in the shadow of the latter. After repeated works on appraisal and exploration of the deposit, its development began only in 2008, which up to now has been carried out in an open pit (Fig. 2).

The host Permian terrigenous and volcanic–terrigenous rocks are represented by flysch interbedding of mudstone and sandstone with interlayers of volcanomictic gravelstone (diamictite). The area of the ore field (Fig. 1), with the exception of several thin (up to 1 m) dikes of intermediate composition, is nonmagmatic. The Vanin stock is known at the NE periphery of the ore field (Sidorov et al., 2010), the outcrop area of which is about 1 km^2. The stock is a complexly structured Jurassic–Early Cretaceous diorite body of the Nera-Bokhapcha Complex, broken by explosive breccia with fragments of the same diorite and gold-bearing quartz, cemented by Late Cretaceous rhyolite. Comparison of the composition of the stock rocks with those of igneous complexes identified by (Palymskii et al., 2015) permits the conclusion that the gold mineralization of the Pavlik deposit is synorogenic.

A large NW-trending tectonic landform is considered the ore-controlling structure (Savchuk et al., 2018), which corresponds to a fragment of the Ten'ka fault zone (Shakhtyrov, 1997). The halos of sulfide (pyrite–arsenopyrite) impregnation and quartz and carbonate–quartz veinlets are predominantly concentrated within en echelon fractures of the footwall of this structure; they are less frequently observed along individual fissures in the hanging wall. The economic gold content has only been revealed in footwall structures. Strike-slip faults steeply (70°–75°) dipping to the east are represented by crush and expansion zones, complicated by a series of subparallel reverse- and normal-fault en echelon fractures. The morphology and spatial position of adjacent fractures at the time of their formation corresponds to right lateral strike-slip paragenesis. The orientation of slickenlines and small offsets along partial fault sutures suggest that early displacements were reactivated in the case of sinistral offsets.

The sampling results revealed several linear ore zones with a NW strike of 300° and NE dip of 40°–70°. Ore mineralization zones consist of combined blocks (from 0.1 to several meters) of weakly and intensely metasomatically and tectonically altered rocks with tectonic crush and mylonitization zones, which contain fragments of boudinaged veins, veinlets, hydrothermal breccia, and fragments with a pyrite (arsenopyrite)–carbonate–chlorite metasomatite–sericite–quartz composition after siltstone. The largest zones, 1 (steeply dipping) and 9 (relatively gently dipping), are traced by the profiles of boreholes and underground mine workings for more than 5000 m along strike and 750 m along dip, with a width of 10–300 m. From the sampling results, orebodies from 1.5 to 7.0 m thick have been identified within ore zones. The ore zones of the Pavlik deposit were opened by a quarry and boreholes to depths of more than 300 m from the surface. The average gold grade in the ore is 2.61 g/t; in rich areas, up to 10 g/t. The gold–silver ratio is 4.35 : 1. The gold distribution is uneven. The gold reserves of the Pavlik deposit are 185.9 t (ore reserves of 7.12 mln t of ore with an average gold grade 2.61 g/t or about 6 mln gold oz). Annual production fluctuates around 6.5 t. Ore is proccessed by conventional gold extraction technologies: gravity, flotation, and sorption leaching (according to data at www.arlan.ru).

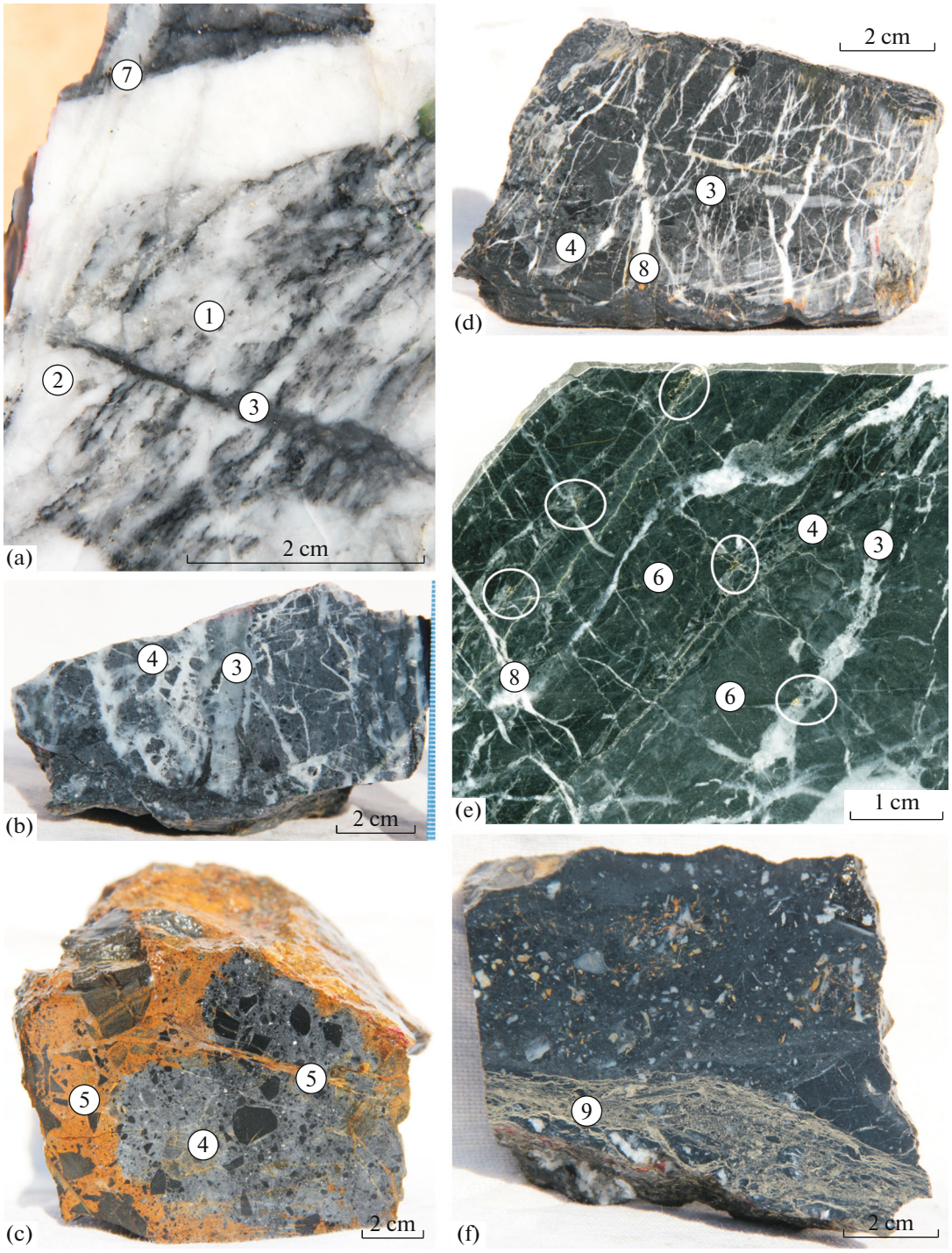

Fig. 3. Typical ores of Pavlik deposit. (a) sample PLK108_1 (Au = 0.12 g/t). Early quartz vein with relict carbonaceous matter (1) intersected by vein of milky white quartz with albite (2). Vein with gray quartz and disseminated arsenopyrite (3) crosscuts early veinlets with displacement (sinistral shear or reverse fault) and in turn is intersected by vein of translucent chalcedony with voids filled with plicated quartz (7). Arsenopyrite develops along suture seams made of carbonaceous matter in quartz (1). (b) Sample PLK108 (Au = 8.1 g/t) and (c) sample. PLK110 (Au = 2.6 g/t), relationships between arsenopyrite–quartz–siltstone breccia (4), productive gray quartz with arsenopyrite (3), and quartz–ankerite breccia and veins (5). (d) Sample PLK109 (Au = 0.48 g/t), veinlets of productive gray quartz with arsenopyrite (3 and 4) and disseminated arsenopyrite intersected by late veinlets and ultrafine stringers of calcite (8); (e) sample PLK146 (Au = 13.7 g/t), relationships between gold-bearing (areas with native gold segregations) quartz–sericite–carbonate microveinlets (6), layered veinlets of arsenopyrite–quartz–siltstone breccia (4), gray quartz veins (3) and late veins with calcite (8); (f) Sample PLK101 (Au = 0.82 g/t), silicified and impregnated with sulfide impregnation of mylonite, crosscut by late netlike vein of fine-grained pyrite (9).

The ore is a mineralized crush zone in siltstone with pyrite phenocrysts, less frequently arsenopyrite and quartz, quartz–carbonate and pyrite(arsenopyrite)–quartz veinlets (Fig. 3). In the shear zone, boudins of multistage quartz veins are widespread (Fig. 3a), along with gold-bearing breccia with siltstone fragments in quartz and ankerite–quartz cement (Figs. 3b, 3c). The morphological features of clasts in breccia do not contradict the hypothesis that such breccia formed during hydraulic fracturing. The ore textures are streaked and disseminated (Figs. 3b, 3d–3f). The sequence of vein formation, indicated by numerals in Fig. 3, is individual for the Pavlik deposit and does not completely coincide with that established by us at other gold–quartz objects (e.g., Aristov et al., 2016).

Among the ore minerals, ilmenite and various sulfides have been identified, in addition to native gold, titanite, and rutile. The total amount of sulfides in ores is no more than 2.0%. Arsenopyrite and pyrite of the synore assemblage account for at least 95% of the total amount of sulfides; up to 5% of sulfides represented by pyrrhotite, sphalerite, chalcopyrite, fahlore, and galena are even less common. According to (Sotskaya, 2017), traces of jamsonite, boulangerite, silver selenide, and scheelite have been found.

In geological features (position in a large transpressional shear zone, lack of direct relationship with granitoid intrusions, and age between the initial (diorite) and final (leucogranite and rhyolite) magmatism of the orogenic stage in the evolution of the territory), the deposit corresponds to an orogenic gold deposit (after (Goldfarb et al., 2005)). In composition of the productive mineral assemblage, the deposit can be attributed to polymetallic gold–quartz objects (after Gamyanin, 2001). The closest analogs of the Pavlik are the Natalka and Degdekan deposits in the same Omchak ore–placer region. The small amount of quartz in the composition of ores (the SiO_2 content in ores rarely exceeds 67%) makes the Pavlik ores closer to those of the Drazhnoe (Yakutia) and Bakyrchik (Kazakhstan) deposits.

METHODOLOGY

To isolate native gold, 89 crushed samples were taken, each weighing about 8 kg. Of these (Fig. 4), 29 samples from orebodies in the open pit, 56 samples from borehole cores in the central part and on the southeastern flank of the deposit, and four samples in the exo- and endomorphic contacts of the Vanin stock. To analyze the fineness of native gold, we used the results from a total analysis of 44 samples weighing up to 300 kg, provided by the Pavlik Gold Mining Company.

Field processing of the selected material included the following:

1, sampling of chips for preparing transparent polished thin sections; 2 , comminution (up to 2 mm) and partial abrasion of samples. To reduce mechanical impact on free large native gold, abrasion was carried out for 0.5 min with a standard duration of 10 min, which made it possible to partially free thin native gold and preserve a significant amount of nonabraded material, +0.1 mm; 3 , selection and abrasion of samples for assay, X-ray fluorescence and mass spectrometry (ICP-MS) analyses; 4, weighing of samples; 5, washing of abraded material on a concentrating table with isolation of gravity concentrate (gray concentrate); 5, selection from tailings; 6, weighing of concentrate; 7, manual finishing of the concentrate with visual monitoring.

After finishing and drying of the concentrate, it was viewed under a binocular microscope to determine the quantitative ratios and morphological features of the main sulfides (pyrite and arsenopyrite) and native gold; native gold and sulfide monofractions were selected, the amount of gold grains and ore minerals were counted, and their linear dimensions were determined. When there was a sufficient amount of native gold, it was weighed on a torsion balance; if weighing was not possible, it was estimated using crossplots. Then, to prepare sections for SEM and microprobe analyses, gold particles with mechanical deformation traces were removed from the samples. Traces of deformations included fresh grooves on the surfaces of gold grains, traces of hammering on the surface, twisting of individual grains into wires or tubes, and heterogeneous contamination of gold grains with mechanical impurities (fragments of arsenopyrite or quartz of different size).

The assay results were obtained in office conditions for all samples. For the boreholes, the results of routine testing by the Pavlik Gold Mining Company (assay analyses) were used; for 19 samples from the quarry, the results of assay analysis carried out by the standard method at the laboratory of TsNIGRI (Central Research Institute of Prospecting for Base and Precious Metals) (analyst T.V. Puchkov).

To determine the natural mineral assemblages of native gold and clarify its main morphological features, transparent polished thin sections were prepared from chips taken from samples with a high gold content, which were then examined and described.

The morphological features of native gold and its relationship with other minerals were clarified by photographing individual gold and sulfide grains glued to adhesive tape, as well as mounted and transparent polished sections in secondary and backscattered electrons on a JSM-5610LV scanning electron microscope (SEM) (Japan). All sections were preliminarily sputtered with a carbon coating. Sulfides, vein minerals, and native gold were identified by semiquantitative determination of their chemical composition on an energy dispersive analytical spectrometer (INCA-

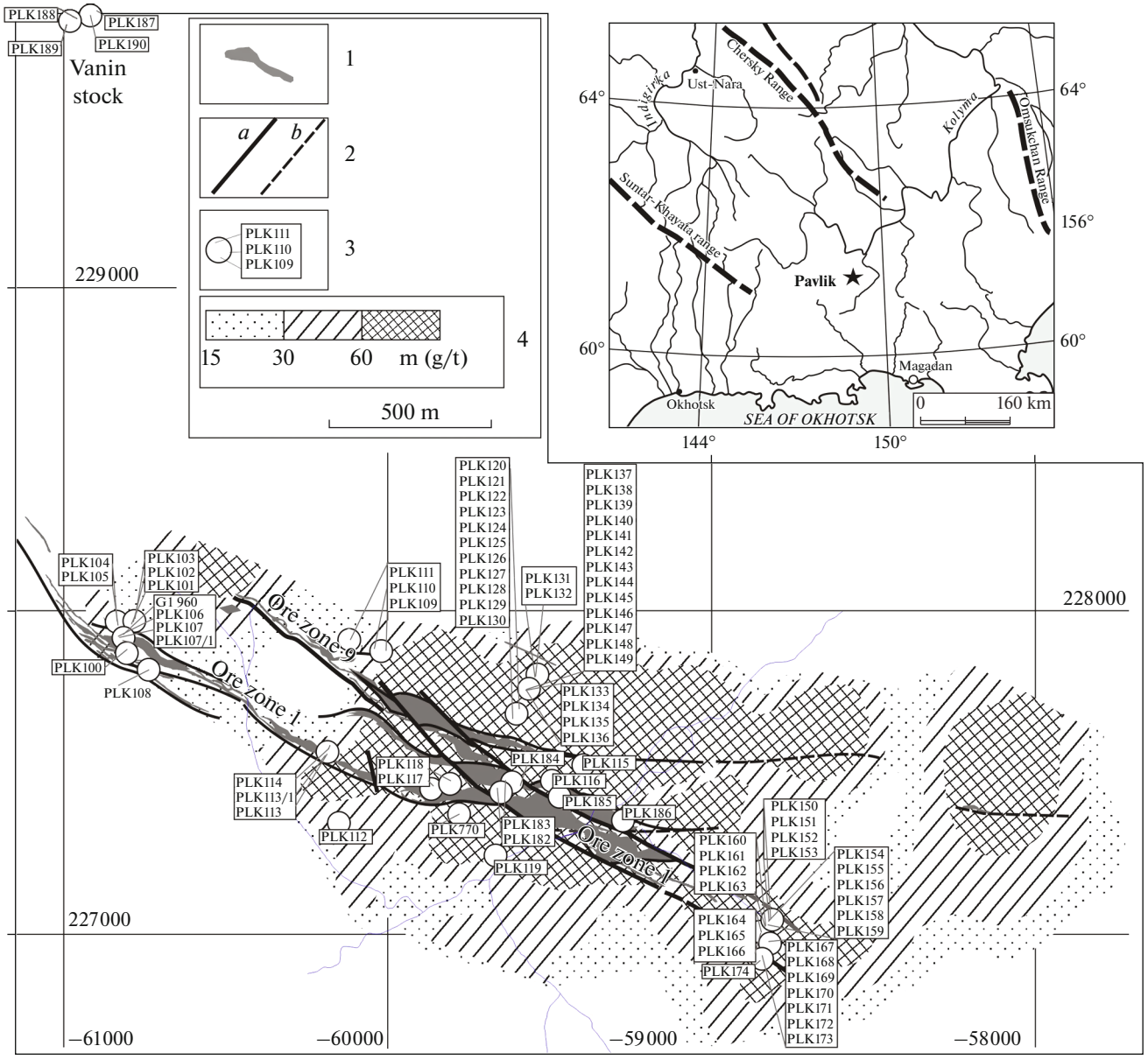

Fig. 4. Sketch map of sampling points at Pavlik deposit site. (1) ore zones and bodies; (2) faults: confirmed (a) and inferred (b); (3) IGEM RAS sampling points (numbered); (4) linear productivity of ore zones by boreholes (m g/t) (from data of V.A. Sidorov). Inset: geographic position of deposit.

Energy 450, UK) (EDS). The analysis was carried out at a point with a locality of 7 μm for a light matrix and 1 μm for elements with large atomic numbers. This was done according to the standard PhyRoZ procedure, at an accelerating electron beam voltage of 25 kV, and a radiation sampling angle of 450°, using an INCAx-sight SDD detector with a resolution of <133 eV and a built-in set of standards. The content of trace elements in native gold was determined along the line *Lα*. For analyses of unpolished samples, the amounts were normalized to 100%. Photography and analyses were carried out by L.O. Magazina at the laboratory of mineral crystal chemistry of IGEM RAS.

The character of the internal structure of gold grains was determined at TsNIGRI by S.V. Yablokova and L.N. Shatilova with etching of polished gold sections by Cr_2O_3 dissolved in HCl.

Categorization of the relationship between gold grains and host rocks and sulfides, as well as identification of inhomogeneities in their internal structure was done in polished sections (checkered and thin sections) with photography in backscattered and secondary (SE) electrons and characteristic X-ray mapping on a JEOL-JXA-8200 microprobe. The contents of major and trace elements in sulfides and native gold

were measured with a JXA-8200 electron probe microanalyzer according to the standard method (EDX) (laboratory for analysis of mineral matter, IGEM RAS, analysts E.V. Kovalchuk and S.E. Borisovsky). The analysis was carried out with an accelerating voltage of 20 kV, a Faraday cup current of 20 nA, and a sampling spot diameter of 1 μm. The exposure time was 20 s. The WDS detector had a resolution of <133 eV. Corrections were calculated by the ZAF correction method with JEOL software. The Au impurity content in pyrite and arsenopyrite was also determined on a JEOL JXA-8200 using a precision technique (Kovalchuk et al., 2017) (increased exposure time).

To determine low Au concentrations in sulfides, we used LA-ICP-MS on an XSeries2 quadrupole mass spectrometer with a NewWave213 laser system. The scanning rate was 15 Hz; the laser energy, 5–7 J/cm^2. The isotopes S33, V51, Mn55, Co59, Ni60, Cu65, Zn66, Ga69, Ge72, As75, Se77, Mo95, Ag107, Cd111, In115, Sn118, Sb121, Te125, Au197, Hg202, Pb208, Bi209, which were selected after (Plotinskaya et al., 2017). The LA-ICP-MS detection limit for gold was 0.01 g/t with a sampling spot size of D = 30–80 μm. The detection limits for other elements are shown in the tables.

To identify invisible gold, LA-ICP-MS analysis was carried out in the profile version for some arsenopyrite and pyrite grains. Pyrite grains were scanned both across the visible sections with 40-μm-wide linear profiles at a rate of 5 μm/s and over an area (about 80 μm in diameter) with a time delay of 95 s (to depth). Each analysis was preceded by a 30-s recording of the noise signal. The MASS1C-USGS commercial standard was used as the benchmark sample. Instrument drift was corrected according to the Fe57 internal standard. Calculations were performed with Iolite 2.5 software. All LA-ICP-MS analyses were performed at the laboratory for analysis of mineral matter at IGEM RAS (analyst V.D. Abramova).

For a composite (gross) sample, the composition of native gold was determined at the TsNIGRI laboratory by ICP-MS on an ELAN 6100 device (a detailed description of the method can be found in (Nikolaeva et al., 2013)).

MAIN RESULTS

Mineral Assemblages

The study of veinlet intersections, mineral relationships, features of mineral grain boundaries, as well as ideas on possible equilibria of minerals under certain physicochemical conditions, made it possible to identify several mineral assemblages and order them relative to the time of ore mineralization. There is insufficient evidence that the identified mineral assemblages were in equilibrium. The compositions of these assemblages contain a number of recurring paragenetic mineral assemblages (e.g., quartz + carbonate + chlorite, quartz + albite, arsenopyrite + pyrite, pyrite + sphalerite), which is unsurprising: deposition ceased after the available space healed, then continued after each tectonic displacement. Equilibrium was repeatedly disturbed due to the change in *PT* conditions, not due to changes in the fluid chemical composition.

The *earliest* mineral assemblage includes white quartz, fragments of which are noted in tectonites (Fig. 3a), sometimes fractured and cemented by late quartz with ankerite and sulfides. Banded quartz textures suggest the development of these veins parallel to cleavage planes.

All later veinlets crosscut regional cleavage (Figs. 5e, 5g).

The earliest assemblage includes veinlets and metasomatites of albite–ankerite–quartz composition with titanite (Figs. 5a, 5e, 5f) and chlorite–hydromica–quartz composition with ilmenite and rutile. The criterion for assigning vein formations to pre- and synore assemblages is the presence/absence of Ti minerals together with albite.

The *synore assemblage* (the time of formation of minerals in the assemblage partially or completely overlaps the formation of minerals of the productive (gold-bearing) assemglage) includes veinlets and metasomatites of pyrite(arsenopyrite)–carbonate–chlorite–sericite–quartz composition (Figs. 5c, 5d, 5f, 5g). Quartz–carbonate–sericite(±potassium feldspar), quartz–carbonate (chlorite)–albite–sericite, and quartz–carbonate–albite metasomatite varieties (facies) are the most clearly distinguished. Breccia with fragments of host rocks and early quartz with varying degrees of tectonic roundness were established in all uncovered horizons and throughout the ore zones. The fragments were cemented and partly replaced by quartz, albite–quartz, and ankerite–quartz cement (Fig. 5d).

The amount of sulfides of the synore assemblage makes up about 95% of all sulfides in the deposit. The amount of arsenopyrite in different samples varies from 5 to 80%, and pyrite, from 20 to 99%. Arsenopyrite and pyrite are observed in disseminated halos in metasomatites after siltstone and tectonite; in thin quartz, ankerite–quartz veinlets; mineralized breccia of siltstone with quartz and ankerite–quartz cement is also encountered. The earliest iron sulfides are represented by disseminated framboid metasomatic pyrite replacing consedimentary carbonates (Fig. 5b); the most recent are microgranular pyrite aggregates in veinlets with chalcedony-like quartz (Figs. 3f, 5g). Some veinlike pyrite grains contain native gold inclusions (Fig. 5g).

Unlike pyrite, which is widespread throughout the entire area of the deposit, arsenopyrite tends to the axial parts of ore zones. Analysis of the relationship with pyrite shows that arsenopyrite forms separate blocks in heterogeneous pyrite metacrystals (Figs. 5c, 5e), traps early pyrite crystals during growth (Fig. 6a),

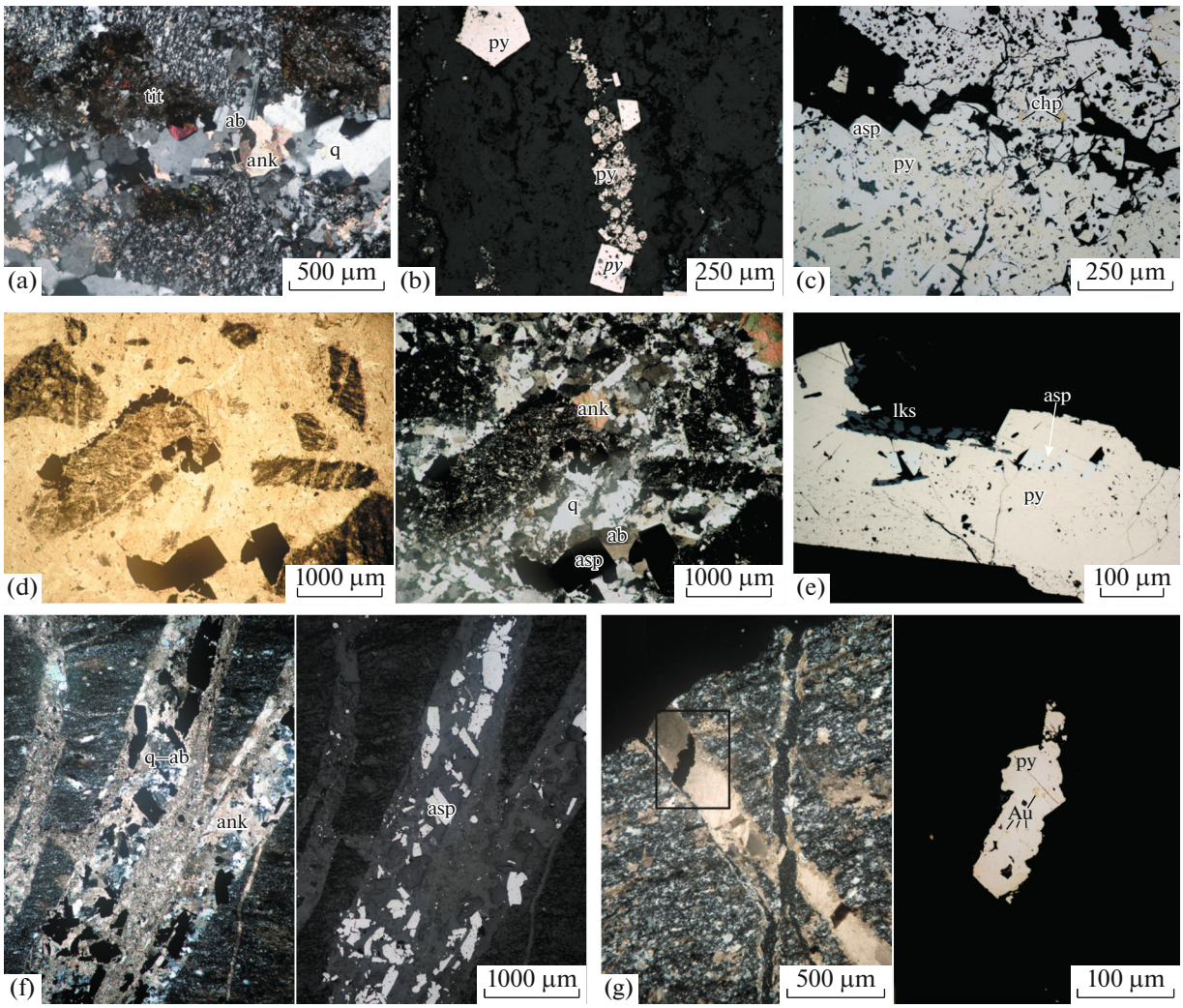

Fig. 5. Pre- and synore mineral assemblages of Pavlik deposit.(a) impregnation in host siltstones and titanite (tit) crystal in selvage of albite (ab)–quartz (q)–ankerite (ank) veinlet (2 in Fig. 4), transparent polished thin section PLK-119, transmitted light, nicols+ ; (b) framboid and subeuhedral pyrite (py) in ankerite–quartz–albite metasomatite with titanite, transparent polished thin section PLK-132, reflected light, nicols=; (c) intergrowths of pyrite (py) metacrystals with heterogeneous (block) structure closely intergrown with arsenopyrite (asp) and with inclusions of chalcopyrite (chp) along cracks, transparent polished thin section PLK-119, reflected light, nicols=; (d) breccia (4 in Fig. 4) of silicified and sericitized siltstone with albite (ab)–quartz (q) cement, replaced by carbonate (ank). Judging from induction boundaries, growth of well-formed arsenopyrite (asp) crystals occurs almost simultaneously with growth of albite and quartz. Transparent polished thin section PLK-117, transmitted light: nicols =, +; (e) metasomatic growth of pyrite–arenopyrite impregnation: pyrite metacrystals overgrow arsenopyrite in quartz–carbonate vein (3 in Fig. 3) with arsenopyrite and leucoxene (lks), transparent polished thin section PLK-141, reflected light, nicols=; (f) albite–quartz–carbonate veinlets (3, 4 in Fig. 4) with ore minerals crosscut cleavage, accompanied by thin, substantially carbonate en echelon veins, transparent polished thin section PLK-143, transmitted light, nicols+ and reflected light, nicols=; (g), aggregate of pyrite crystals connects filamentary sericite–carbonate veins (6 in Fig. 4), crosscuts carbonate vein (5 in Fig. 4) and is subparallel to late micrograin quartz vein (7 in Fig. 4). Pyrite contains fine gold impregnation. Transparent polished thin section PLK-125, transmitted light, nicols=, +, examined area, reflected light, nicols=.

and grows pyrite crystals; ultimately, pyrite grows arsenopyrite crystals (Figs. 6d–6f). Based on these relationships, it can be concluded that the duration of arsenopyrite crystallization is shorter than that of pyrite crystallization. Judging from the composition of inclusions in arsenopyrite from ore zone 1 (Fig. 6a), the solutions from which arsenopyrite is formed are not in equilibrium with the host rocks. While pyrite hardly undergoes any alteration during arsenopyrite crystallization, host rock minerals containing calcium or magnesium (dolomite–ankerite, apatite) are replaced or partially dissolved. Analogs of the synore assemblage were observed on the northern flank of the deposit, in the Vanin stock's zone of influence. Arsenopyrite hosts lellingite and bismuth telluride impregnation (Fig. 6b).

The growth of metasomatic crystals with a large number of relict host rocks and, partially, well-formed

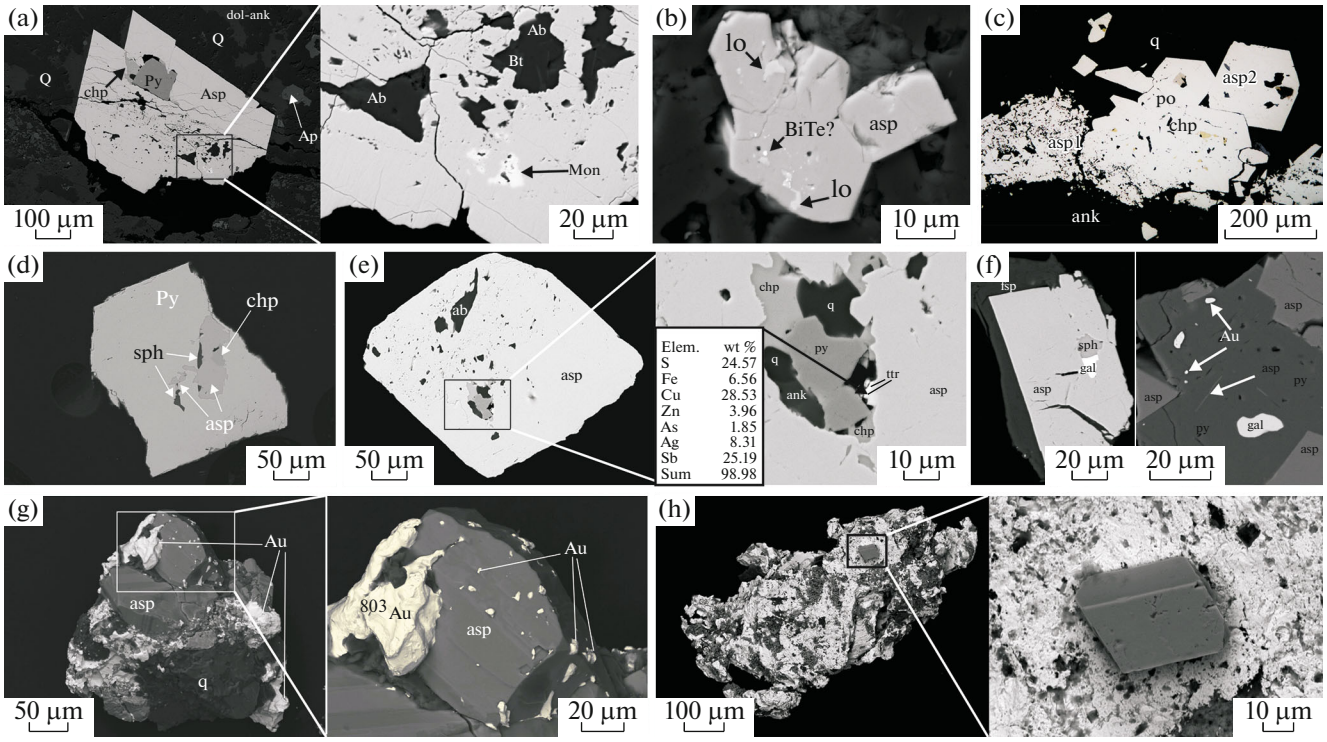

Fig. 6. Ratios of arsenopyrite with minerals of auriferous (productive) assemblage, (a) PLK185. Metasomatic growth of arsenopyrite (asp) into albite (Ab)–sericite (ser)–dolomite–ankerite (siderite) (dol–ank)–quartz (Q) microgranular aggregate with apatite (Ap) segregations and pyrite (py) impregnation. Monazite (Mon) is formed in arsenopyrite due to apatite, and biotite (bt) due to sericite and siderite. Pyrite relicts are preserved in arsenopyrite. Latest chalcopyrite (chp) grows at pyrite–arsenopyrite boundary; (b) PLK188 (Vanin Stock). The increased temperature during formation of arsenopyrite impregnation in igneous rocks recorded by formation of impregnated lellingite (Lo) and bismuth telluride (BiTe?) in arsenopyrite crystal. (c) PLK123. Fractured arsenopyrite (asp1) contaminated with numerous inclusions in sericite–quartz–carbonate metasomatites and well-formed crystals (asp2) with growth zones and inclusions of pyrrhotite (po) and chalcopyrite (chp) in quartz vein coeval with metasomatites. (d) PLK325. Pyrite grows to arsenopyrite (asp)–chalcopyrite (chp)–sphalerite (sph) intergrowths; (e) PLK770. Arsenopyrite metacrystal (asp) with inclusions of pyrite (py), chalcopyrite (chp), fahlore (ttr), quartz (q), and carbonate (ank). (f) PLK770. Left, fragment of arsenopyrite (asp) crystal with inclusions along fractures of late galena (gal) intergrown with sphalerite (sph); arsenopyrite (asp) intergrown with later pyrite (py), which contains inclusions of galena (gal) and gold (Au). Host matrix is potassium feldspar (fsp); (g) gold forms fine impregnation and veins in arsenopyrite crystal and massive lumpy segregation in interstitial space (PLK770). (h) PLK117. Regular prismatic arsenopyrite crystal overgrows porous surface of native gold. Dissolution sculptures on surface of porous gold. (a, c) transparent polished thin sections. (a) image in secondary electrons (SEM), (c) reflected light; (b, d–f) mounted thin sections, image in reflected electrons (microprobe, analyst S.E. Borisovsky); (g, h) sections from heavy fraction of communited samples, secondary electron image (SEM). Analyst L.O. Magazina.

arsenopyrite crystals in quartz veins starts before pyrrhotite and chalcopyrite crystallization (Fig. 6c). These sulfides, as well as sphalerite, can be found in certain arsenopyrite crystal growth zones and often form induction surfaces with arsenopyrite, indicating simultaneous growth (Fig. 6d). According to the results of studying mounted thin sections from arsenopyrite monofractions, individual arsenopyrite crystals (1–2 arsenopyrite grains per group of 30–40 grains) contain polymineral pyrrhotite–chalcopyrite–sphalerite or carbonate–sphalerite–pyrite–tetrahedrite inclusions (Fig. 6e) and are crosscut by microveins of pyrrhotite, sphalerite, galena (Fig. 6f), or native gold. We attribute polymineral inclusions to syngenetic inclusions arising during growth of arsenopyrite and characterizing the crystallization setting. The established growth of arsenopyrite both before and after crystallization of native gold (Figs. 6g, 6h) suggests that arsenopyrite belongs to the synore assemblage. This is indirectly confirmed by the wide distribution of low-gold-bearing or barren arsenopyrite–quartz veinlets, which were sampled from boreholes.

The *ore* assemblage include microveinlets and impregnations (about 5% of sulfides of the deposit) of pyrrhotite–chalcopyrite–sphalerite composition in synore veinlets and metasomatites. The latest mineral of the ore assemblage is galena (less than 1% of the total amount of sulfides) (Fig. 6f), located in veinlike inclusions in arsenopyrite, sometimes in intergrowths with sphalerite, or isolated inclusions in pyrite. Vein minerals are represented by sericite, chlorite, dolomite–ankerite carbonate, albite, and potassium feldspar. The fact that these minerals belong to the ore

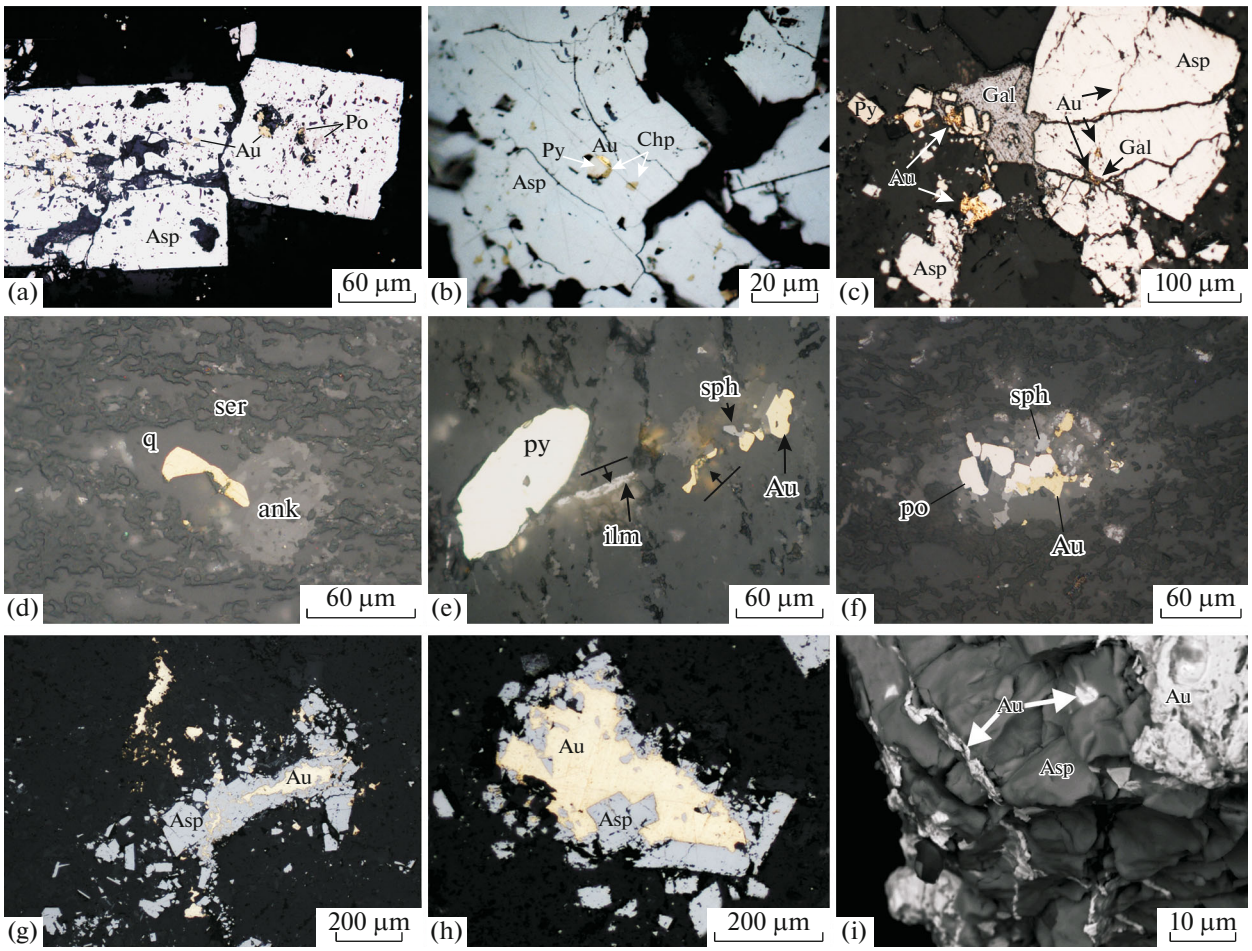

Fig. 7. Forms of segregation and assemblage of native gold (a–c) microscopic finely dispersed and dusty (2–10 μm) gold in sulfides: (a) inpregnation of fine gold (5–10 μm) in cracks in arsenopyrite (asp) with pyrrhotite (po) inclusions (PLK131), (b) inclusions of native gold (4 × 2 μm) intergrown with chalcopyrite (chp) and pyrite (py) in arsenopyrite (asp) (PLK130); (c) veinlets of galena (Gal) with native gold (Au) crosscut arsenopyrite (Asp); in individual cracks in arsenopyrite, gold forms independent segregations. Pyrite (Py) crystals contain gold inclusions and are crosscut by galena veins (PLK146). (d–f) microscopic dusty and fine (10–100 μm) gold in sulfide–sericite–carbonate–quartz metasomatites. (d) gold forms intergrowths with quartz (q) and carbonate (Ca) in microblocks bounded by oriented sericite (ser) aggregates (PLK143); (e) veinlike intergrowths of gold with sphalerite (sph) crosscut fracture with a ilmenite layer (ilm) (arrows show orientation of veinlets) (PLK125); (f) intergrowths of gold with sphalerite (sph) and pyrrhotite (po) (PLK143). (g–i) visible very fine and fine (>100 μm) gold in arsenopyrite and host siltstones: (g) native gold crushes arsenopyrite, forms fine network of veinlets in it, and in interstices of albite–carbonate–quartz aggregates in host rocks again forms massive aggregates (PLK146), (h) massive gold in central part of intergrowth of arsenopyrite crystals (PLK108); (i) finest (from 5 to less than 1 μm) gold stringers (white) penetrate into crushed arsenopyrite (PLK108). (i) photo of grain in secondary electrons (SEM) (analyst L.O. Magazina); remainder, photos of transparent polished sections in reflected light.

assemblage is evidenced by their intergrowth with native gold and inclusions in native gold.

Microscopy established that native gold (up to 0.2% of the amount of sulfides) is disseminated in the form of fine impregnations everywhere in the deposit (e.g., in samples PLK-105 and PLK-770 of ore zone 1 and PLK-143 and PLK-146—of ore zone 9). Submicron native gold is in the form of isolated impregnations in pyrite (Figs. 5g, 6f), in fracture zones in pyrite and arsenopyrite (Figs. 7a–7c), and in quartz–carbonate–sericite aggregates, including intergrowths with carbonate (Fig. 7d), pyrrhotite, chalcopyrite, and sphalerite (Figs. 7e, 7f). Larger veinlike monomineralic segregations of native gold are observed in arsenopyrite with (Fig. 7c) or without veinlets of galena (Figs. 7g–7i) and, less frequently, in carbonate and quartz of altered host rocks (Fig. 7g).

Induction boundaries of simultaneous growth are observed between some segregations of carbonates, pyrite, chalcopyrite, pyrrhotite, sphalerite, galena, and native gold.

The relationships between native gold and arsenopyrite are the most diverse. Native gold forms impregnations associated with fracturing and irregular interstitial segregations; it grows on crystal rims in the form of spongy and crystalline segregations, and cements

(a)

Total weight of samples, kg 14749.7	Grain size (based on 44 samples)						Mean diameter, mm
	2–1 mm	1–0.5 mm	0.5–0.25 mm	0.25–0.1 mm	0.1–0.063 mm	<0.063 mm	
	Weight, mg						
	535.8	8365.0	12495.4	12709.1	2795.1	2409.4	
	%						
	1.4	21.3	31.8	32.3	7.1	6.1	0.3

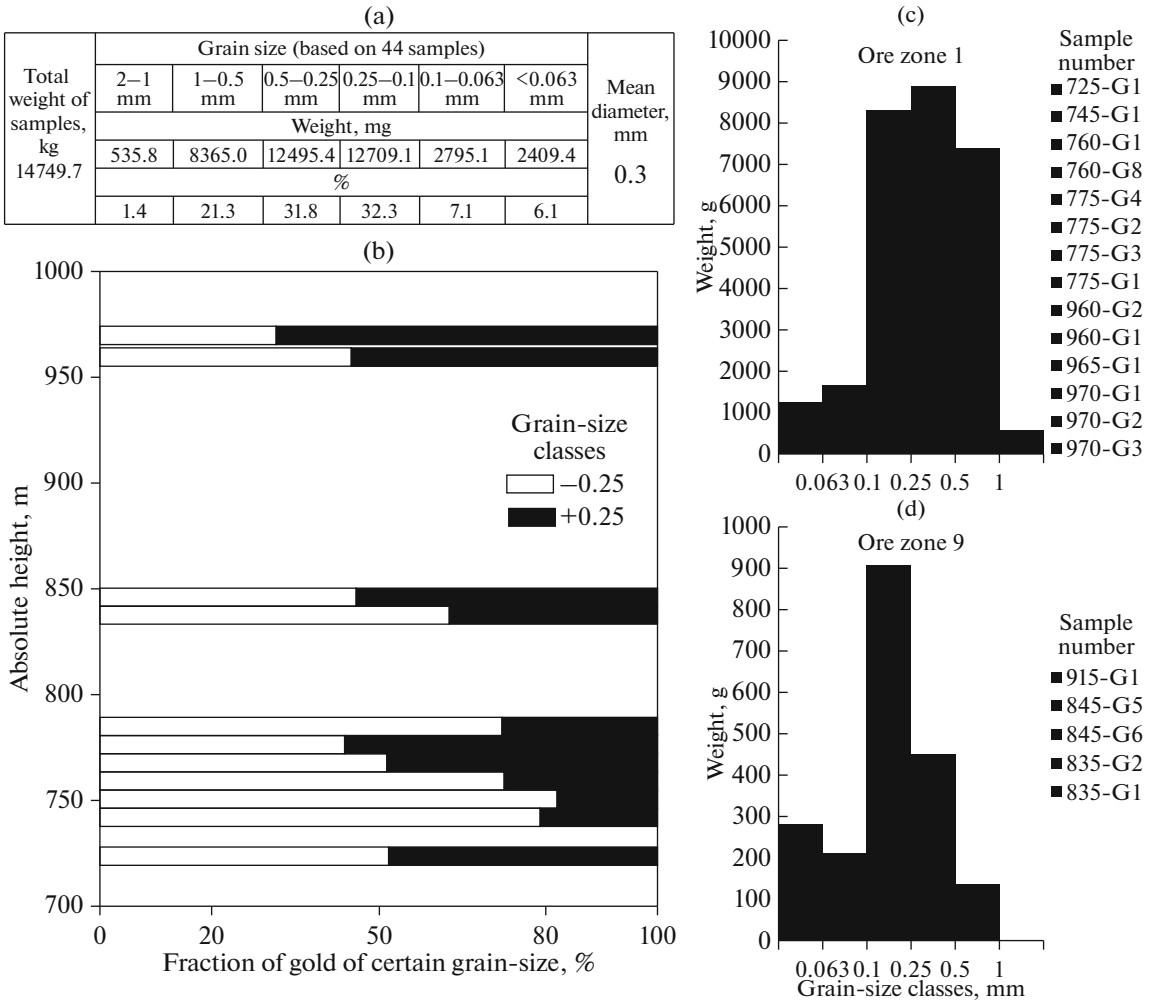

Fig. 8. Gold grain distribution of Pavlik deposit. Results of grain size distribution (sieve) analysis (a), change in relative amount of gold of various dimensions in vertical section along ore zone 1 (b), and distribution of gold grain size in ore zones of Pavlik deposit (c, d).

arsenopyrite fragments. Some gold grains contain fragments of arsenopyrite crystals. The finest native gold veinlets (0.1–5 μm) (Fig. 7i) penetrate into arsenopyrite from segregations of massive native gold, while in the interstices of albite–carbonate–quartz aggregates in host rocks, native gold again forms massive aggregates (Fig. 7g). The appearance of netlike or linear veinlets of native gold is most frequently noted on the periphery of large massive veinlike segregations in arsenopyrite.

The study of the ratio of ore and vein minerals allows us to conclude that the minerals of the ore (productive) assemblage formed during the formation of the synore mineral assemblage.

Native Gold

Native gold was successfully established in 61 of the 89 samples. The gold content in these samples varies from 0.05 (the minimum detection limit for assay analysis) to 19.3 g/t; the average value is 3 g/t, and the content variance is 10.6.

The particle size of native gold established in comminuted samples varies from thousandths of a millimeter to 0.5 mm, rarely to 1.5–4.0 mm.

Counting the number of gold grains of various sizes made it possible to establish that most of them at the Pavlik deposit can be attributed to the following size groups (in accordance with the classification of (N.V. Petrovskaya, 1973)):

1. Microscopic (finely dispersed, dusty, and fine) (peak size at 0.075 mm).

2. Visible (very fine and fine) (size peaks at 0.25, 0.55, and 0.85 mm)

These data fit the grain size distribution data (Fig. 8a) according to which the main contribution to the total weight of gold comes from gold grains of the fine class with an average size of 0.3 mm, and the share of dusty and finely dispersed grades (less than 0.05 mm)

Table 1. Composition of native gold from primary deposits of the Omchak ore–placer cluster, wt %

	Pavlik EDX, (excluding low- and high-grade rims)	Pavlik ICP MS**	Natalka EDX (Pluteshko et al., 1988)	Degdekan EDX (Litvinenko, 2009)
N_Au	59			
N EDX	152			63
Au	73.5–86.7	77.2	73.8–80.2	75.1–83.0
Ag	13.3–23.1	22.1	N.d.	N.d.
Au/Ag	4.17	3.49		
As*	–	0.13	0.005 / 100	0.04 / 37
Hg*	0.2 / 34	0.15	N.d.	0.1 / 29
Zn*	–	0.023	0.015 / 9	N.d.
Pb*	–	0.002	0.07 / 54	0.81 / 71
Cu*	0.06 / 27	0.004	0.004 / 100	0.05 / 54
Te*	–	7×10^{-4}	N.d.	0.2 / 78
Se*	–	N.d.	N.d.	0.02 / 78
Sb*	0.01 / 9	2×10^{-4}	N.d.	0.08 / 57
Bi*	–	9×10^{-5}	sl / 27	0.18 / 32
Fe*	0.93 / 50	0.29	0.03 / 72	0.6 / 62

Sign "–", content of elements below sensitivity of analysis; N.d., data on element content are not given; sl, element content at sensitivity level of analysis.
* In numerator, maximum values; in denominator, occurrence frequency (%).
** Composite (gross) sample for Pavlik deposit. PLK111, PLK112, PLK115, PLK116, PLK119, PLK183, PLK184, PLK185 (charge 13.4 mg).

accounts for 6 to 26%. It should be mentioned that these grain size distribution data were obtained for gravity concentrates and obviously underestimate the amount of microscopic native gold.

Visible native gold predominates in steeply dipping ore zone 1 (Fig. 8c); the amount increases towards the surface. Figure 8b shows histograms reflecting the amount of gold of various dimensions in ore zone 1 at a certain vertical mark. At elevations of 730 and 770 m, the proportion of visible gold (up to 1 mm) increases irregularly, which may be associated with local heterogeneities of the ore-hosting tectonic zone. The amount of native gold more than 1 mm in size remains constant at all horizons (about 1.5%). The predominance of microscopic native gold is observed in shallow ore zone 9 (Fig. 8d). The amount of it grows in the elevation range 770–750 m.

To obtain data for comparison with other primary deposits and placers, the TsNIGRI laboratory carried out bulk analysis (ICP-MS) of native gold from samples collected throughout the deposit. Fe, Hg, and As were detected in the sample in appreciable amounts (Table 1). The Zn content is smaller by an order of magnitude. The Cu and Pb contents are even smaller. Bi is contained in a significantly amount (up to 18 g/t). Elevated Na, Mg, Al, Ti, Fe, and As contents indicate the presence of albite, chlorite, dolomite, rutile, and arsenopyrite inclusions in native gold. The significant amount of inclusions in individual gold grains is confirmed by the fact that the gold fineness in the bulk sample is slightly lower than the median value deter-

Table 2. Variations in composition of native gold from ores of Pavlik deposit EDX, wt %.

Number (elevation, m)	N_Au	N_n	Au	Ag	Au/Ag	Hg	Fe
PLK108 (941)	7	14	81.4–86.7	13.3–17.3	4.7–6.5	0.08 / 21	0.62 / 64
PLK154 (763)	7	14	75.9–81.1	18.3–22.6	3.4–4.4	"–"	0.15 / 57
PLK124 (631)	15	26	78.8–81.3	17.4–19.4	4.1–4.7	0.22 / 36	0.93 / 68
PLK125 (622)	5	11	68.0–79.7	18.8–29.4	2.3–4.2	0.29 / 64	"–"
PLK186 (742)	4	12	79.2–80.3	18.7–19.8	4.0–4.3	"–"	"–"
PLK187 (797, Vanin stock, xenolith)	8	25	76.2–82.0	18.1–22.5	3.4–4.5	0.12 / 36	0.6 / 76
PLK103 (945)	3	15	73.5–98.2	0.44–23.1	2.9–222.1	"–"	0.76 / 13
PLK117 (718)	3	10	75.1–97.8	0.96–23.1	3.3–101.4	0.43 / 50	"–"
Omchak	7	25	72.8–99.3	1–23.8	3.0–99.3	0.5 / 44	"–"

N_Au, number of analyzed gold grains; N_n, number of analyses. EDX measurement error (1σ,%) Hg = 0.04, Cu = 0.03, Sb = 0.05, Fe = 0.07. Numerator contains maximum values (high contents in edge parts of grains are excluded); denominator contains occurrence frequencyof contents exceeding sensitivity level (%). "–", content below analysis error; for Cu and Sb, measured values did not exceed 2σ.

mined by the XRD-measured fineness values at points (the difference is about 35‰).

The chemical composition of native gold at points for individual grains based on the EDS and EDX data is given in an electronic appendix (Appendix 1). Variations in the composition of native gold based on the XRD data are given in Table 2. The main impurity is silver. Sporadically, up to 0.5% (EDX) (4.3% EDS) mercury and 0.06% (EDX) (0.43% EDS) copper has been noted. According to EDS determinations in single samples, the Ni, Pd, Zn contents are elevated. According to the EDX data, the remaining elements are contained in quantities below the minimum detection limit. These differences are explained by the low accuracy of EDS determinations along the $L\alpha$ line. In addition, nearer-surface parts of gold grains were analyzed with EDS; EDX was used to analyze their internal parts. Therefore, only the results obtained for gold and silver based on the EDS data are given.

The average fineness of native gold fluctuates around 800; the median and modal values for the sample coincide, 806‰ (Fig. 9a). The histogram shows three additional fineness peaks. The first peak, with maximum values of about 775, and most intense refers to inhomogeneous native gold in dolomite–ankerite–quartz aggregates. The second, with maximum values of 840–860, was recorded for native gold from ore zone 1 (770, PLK108). Finally, the third peak (980–990) is associated with high-grade rims that developed in tabular native gold. Although the fineness variance even in neighboring gold grains can reach almost 100‰, based on the averaged data (EDS, EDX) for 13 samples from the ore zone 1 (Fig. 9a, inset) and on the entire dataset (EDX) (Fig. 9b), there is an overall poorly expressed tendency toward growth in fineness from bottom to top in the vertical section of the field. This tendency is violated in samples from zone 9.

Morphological Features of Native Gold

Finely dispersed (1–5 μm) and dusty gold grains (10–50 μm) are characterized by jagged or even borders and a tabular or droplike shape (Figs. 5, 6, 7). In most cases, such gold grains are isolated within sulfides or in microblocks composed of quartz and carbonate and bounded by oriented sericite aggregates. The composition and morphology of these gold grains are uniform, but their quantity and distribution are most important for improving technological processes, since neither finely dispersed native nor dusty gold can be completely freed with standard grinding of ores, and in a gravity–flotation ore processing scheme, they end up in tailings.

Thin (50–100 μm), very fine (100–250 μm), and fine (250-1000 μm) native gold is most often observed in selvages of quartz veins and veinlets and in crush and foliation zones of host rocks and arsenopyrite. Native gold of this fraction is extracted in a gravity

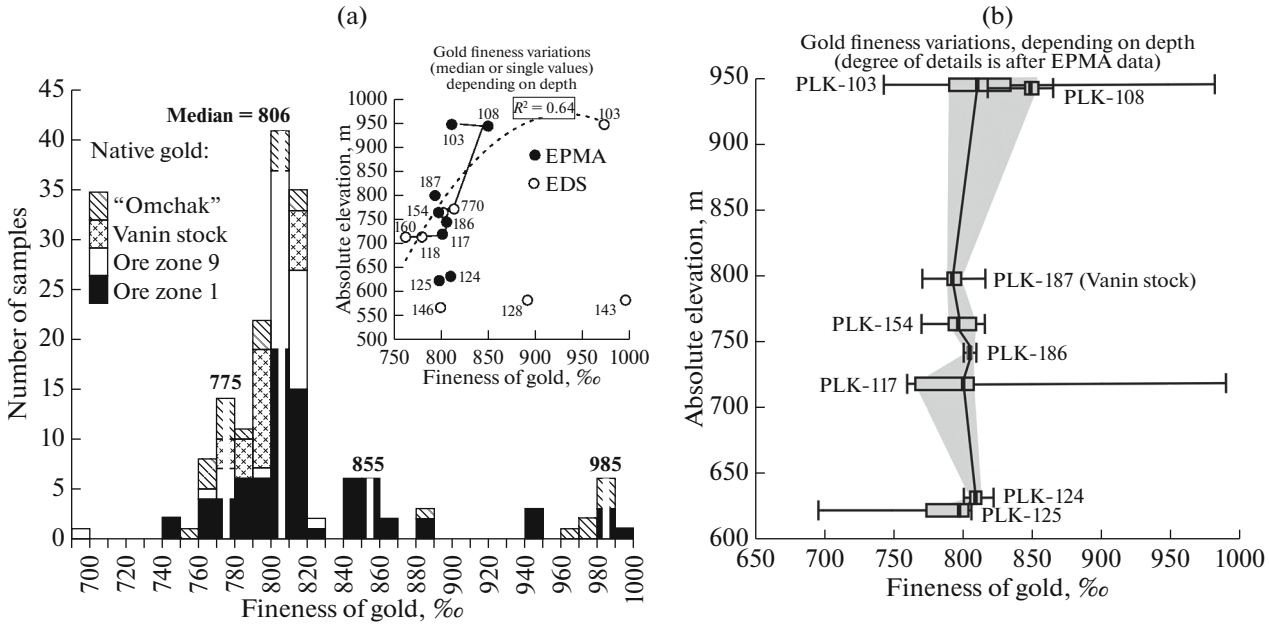

Fig. 9. Fineness variations of gold from ores of Pavlik deposit. (a) histogram of gold fineness (EDX); inset: variations in fineness (median or single values according to EDX and EDS data) in vertical section, R2, reliability value of approximation of data for ore zone 1 by curve of second-degree polynomial; (b) categorization of variations in fineness in vertical section (data of the EDX). In "box&whisker" diagram: horizontal line indicates range of values; diagonal hatching indicates minimum, median, (connected by lines), and maximum values. Central quartiles (50% of values) are shown with rectangles and are connected by shaded fields.

concentrate; it is this gold that is of prospecting value, since it accumulates in placers. Let us consider the morphology of native gold of this fraction in more detail.

Massive pseudocrystalline, fracture–vein–like and lumpy morphological types (after *Samorodnoe ...*, 2015) of extremely fine and fine native gold is ubiquitous and predominantly abundant (Figs. 10a, 10b). Octahedra and spherical formations were found in only two samples. Other forms have features by which one can judge certain gold formation conditions:

Lumpy-porous native gold. The massive central part of gold grains is gradually replaced by a porous periphery (Fig. 10c, d). The rims of grains often curl up. Sometimes pseudocrystalline areas with a smooth surface are observed (Fig. 10c). Native gold with this morphology is common both in the northwestern (PLK117, PLK118) and central and southeastern (PLK154, PLK157, PLK770) parts of the field. As a rule, spongy-porous native gold is associated with arsenopyrite mineralization, which is confirmed by numerous intergrowths of this gold with arsenopyrite. The share of native gold of this morphological group is about 15% of the total .

Platy (tabular) native gold is represented by flattened rounded or oval platelets (Figs. 10e, 10f) of reddish color. The ratio of the average diameter of the platelets to the thickness is ≥10; the surface is finely shagreen. They differ sharply from other gold grains by their round or oval shape, as well as by the color and character of the surface. Most Kolyma placer gold researchers classify such grains as perfectly rounded (Shilo, 2000), but we noted them at different slice levels of the ore zones 1 and 9, both in boreholes (PLK143, 154) and in the open pit (PLK185, 186). A number of tablets are encountered in ores of the central part of the deposit, as well as in placer halos around it. The share of native gold of this morphological group does not exceed 1.5% of the total .

Features of the Surface of Gold Grains, Inclusions in Native Gold, and Heterogeneity of Native Gold

The character of the surface of gold grains (sculpture marks on gold grains and porous surfaces) in metasomatites is determined by the peculiarities of the host setting (growth in the interstitial space), while in arsenopyrite, it is governed by features of fractures developing in sulfide, which are filled with native gold during or immediately after formation. During oxidation and further removal of arsenopyrite, netlike vein aggregates result in a spongy surface of gold grains in placers. The surface of the largest native gold grains is of the same type, but not uniform. The pitted surface of native gold with smooth pit walls is caused by imprints of carbonate, quartz, sericite, and arsenopyrite crystals. The size of the pits is comparable to that of gold grains (Figs. 10a, 10b). Host minerals can be preserved in native gold as inclusions with clear crystallographic outlines (Figs. 11a, 11b). A combination of smooth and porous irregular areas is observed, as

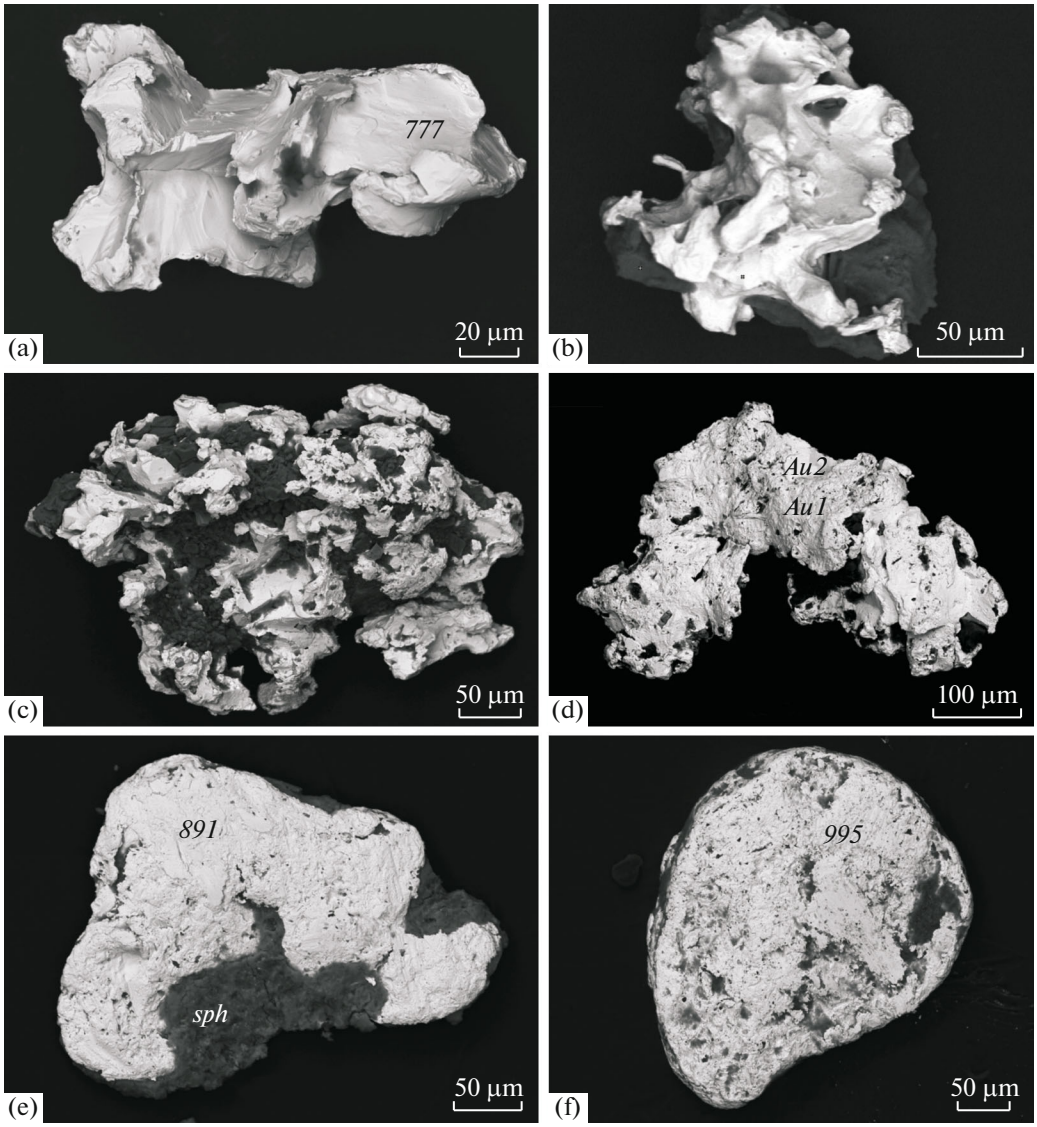

Fig. 10. Features of morphology of visible (>0.2 mm) gold. (a–d) irregular cementation and interstitial forms: (a) interstitial massive gold with imprints of quartz, albite, and carbonate crystal facets (PLK770); (b) fractured with fragments of porous gold, filling intergranular space (PLK770); (c) hemidiomorphic lumpy gold with fragments of crystalline gold (PLK157); (d) cementing lumpy gold intergrown with spongy-porous gold (PLK-154); (e–f) fractured tabular gold (Omchak type) with a high-grade surface: (e) intergrowth with sphalerite (PLK-128), (f) intergrown with chlorite (PLK-143); on the surface, late slickenlines. Photo of grains in secondary electrons (analyst L.O. Magazina).

well as porous microsculpture of the surface with microgrooves and numerous imprints of other minerals. In some cases, on the surface of native gold segregations, imprints of slickenlines from the walls of ground surfaces where native gold crystallized are observed (Fig. 11g). Spongy-porous native gold with a large number of nodes and micropores on the surface (up to 20 pores/100 μm^2) develops on the periphery of massive native gold segregations (Figs. 11f, 11g). About 15% of pores differ in size (2–3 μm) and depth. Some contain carbonates and sericite. A smooth surface with imprints of other minerals and relatively coarse (2–3 μm) is rare (1–2 pores/100 μm^2); pores are less common (Figs. 11a, 11e).

Some native gold grains contain relatively large inclusions of pyrite, arsenopyrite, quartz, carbonate, albite, potassium feldspar (K feldspar), sericite, chlorite, and sphalerite. Monomineralic aggregates and sometimes single crystals of sericite, albite, carbonate, arsenopyrite, and less frequently K-feldspar, fill voids in native gold, grow together with gold grains, or their acute-angled fragments are cemented with native gold (Figs. 11b–11d, 11g–11i). Each isolated inclusion is filled with either sericite or albite, and sometimes

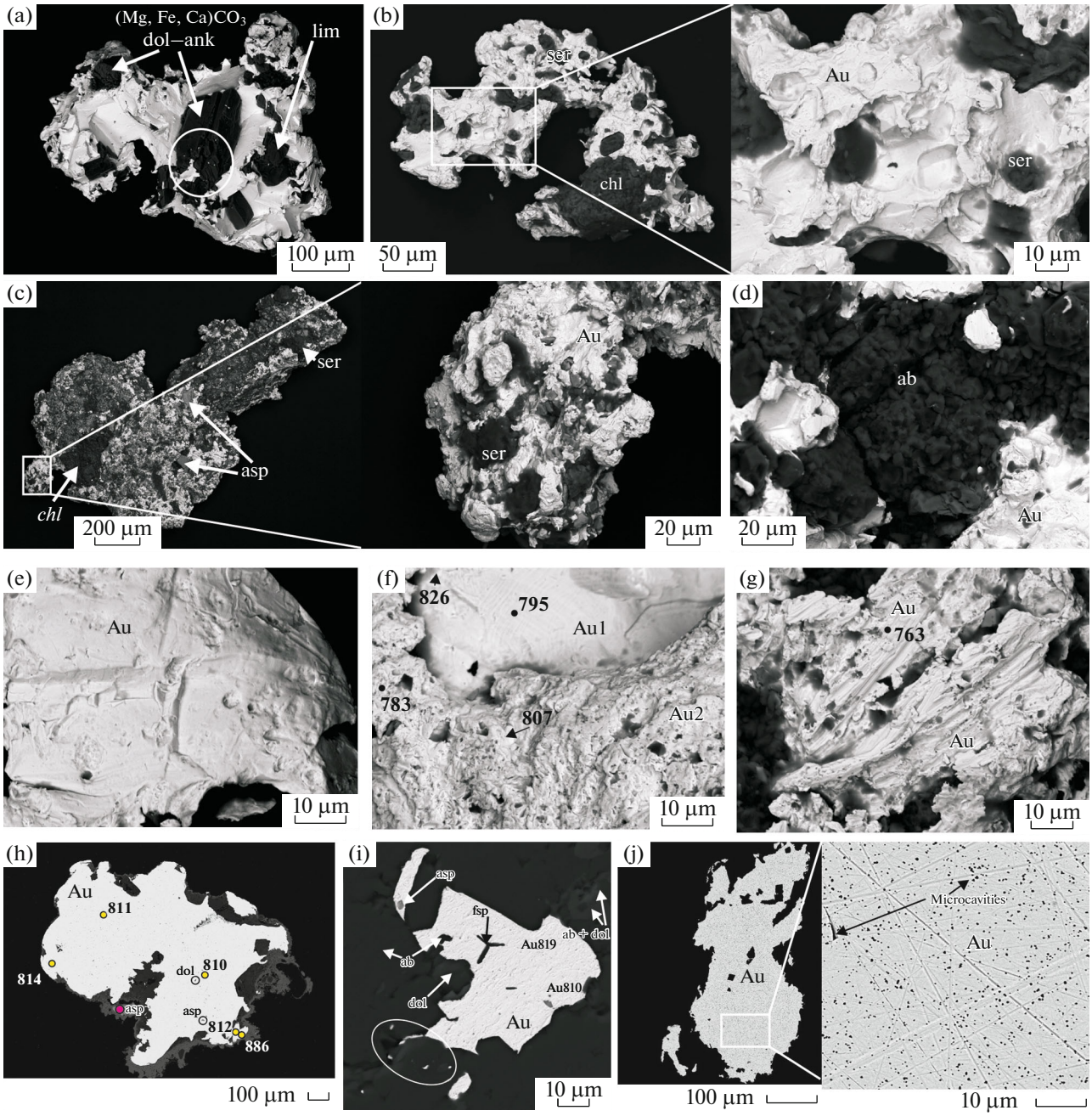

Fig. 11. Intergrowths of native gold with vein minerals and inclusions in gold. (a–d) visible very fine (>100 μm) interstitial and cementat massive and spongy-porous native gold intergrown with dolomite–ankerite (ank), (white circle in Fig. 11a demarcates carbonate with microinclusions of native gold (a)), sericite (ser) and chlorite (chl) (b); with arsenopyrite and chlorite (c); albite (ab) (d); (e–g) surface of interstitial gold: (e) smooth surface with imprints of crystals of vein and ore minerals; (f) spongy-porous gold with rough surface on periphery of massive segregations of gold with smooth surface; (g) casts of preore slickenlines on porous gold. (h–j) microinclusions in gold. (h) gold grain with rare inclusions of carbonate (dol) and arsenopyrite (asp) fragments, small black dots, microinclusions (mostly voids) (50–60 per 100 μm^2); and, (i) gold grain in interstitial space of albite–dolomite metasomatite contains inclusions of potassium feldspar (fsp). Inclusions of albite (ab) and arsenopyrite (asp) in gold (Au) have clear crystallographic facets, which may indicate their trapping in solid state. Internal structure of gold grain is characterized by development of microvoids (~30 per 100 μm^2). Micron-sized imregnation of gold is developed around large segregation (circled); (j) gold grain from xenolith of quartz vein in explosive breccia of Vanin stock is saturated with numerous microinclusions; inset shows that these are predominantly voids 0.1–0.5 μm in diameter with average density of 39–40 per100 μm^2; (a–g, i) images in secondary electrons (SEM, analyst L.O. Magazina); (a–g) sections of grains on scotch tape; (a, c, e, g) sample PLK118; (b) sample PLK157; (d, f) sample PLK154; (i) transparent polished section PLK103; (h, j) images in backscattered electrons (analyst S.E. Borisovsky); mounted thin sections.

Table 3. Some statistical characteristics of fineness of native gold from Pavlik deposit depending on analytical methods, position of samples in space, and for individual samples

Analysis type	Sampling site	Elevation, m	N_Au	N _n (weight, g)	Variance	Fineness*	Quartile_1	Quartile_3	Min	Max
EDX	Pavlik		59	152	2671	806	792	815	697	990
EDS	Pavlik		34	45	2221	804	792	825	762	995
EDS + EDX	**Pavlik**		**93**	**197**	**2558**	**806**	**792**	**816**	**697**	**995**
ICP MS	Combined sample			(0.013)		**771**				
EDX	Center of deposit		44	102	1950	807	802	816	697	990
EDX	"Omchak"		7	25	7500	804	778	889	753	990
EDX	PLK187	797	8	25	174	793	790	799	772	817
EDS + EDX	1 zone		67	146	**2382**	**807**	**793**	**844**	**744**	**990**
EDS + EDX	Zone 9		26	51	**1236**	**806**	**802**	**811**	**697**	**995**
Ore zone 1										
EDX	PLK103	945	3	15	4114	811	791	835	744	982
EDS	PLK103	945	1	1		972				
EDX	PLK108	941	7	14	155	849	845	855	819	866
EDX	PLK117	718	3	10	9237	801	766	912	761	990
EDS	PLK118	712	1	1		779				
EDX	PLK154	763	7	14	201	797	790	810	771	816
EDS	PLK154	763	2	4	276	802	793	810	780	819
EDS	PLK160	712	1	1		762				
EDX	PLK186	742	4	12	6	805	804	806	801	809
EDS	PLK770	770	23	24	1117	813	792	835	774	884
Ore zone 9										
EDX	PLK124	631	15	26	26	810	806	814	802	823
EDX	PLK125	622	5	11	1043	798	774	805	697	806
EDS	PLK128	580.7	1	1		891				
EDS	PLK143	581.2	1	1		995				
EDS	PLK146	566	4	12	112	799	793	810	784	817

*, median value or calculated from a single measurement.

Fig. 12. Features of internal structure of gold. (a–c) most widespread veinlike homogeneous (fineness variance in samples from 26 to 155), single-crystal (?) gold grains. (a) (sample PLK124) intergrown with arsenopyrite; a1, photo of etched grain in reflected light; a2, in secondary electrons (802–806); (b) (PLK146) photo in secondary electrons: b1, streaky monocrystalline (fineness 804–817) intergrown with quartz and dolomite–ankerite; b2, small mottled heterogeneities in gold (790–793) with arenopyrite inclusions; (c) (PLK108), homogeneous veinlike in arsenopyrite, veinlets from massive to thin: b1, photo of etched grain in reflected light; b2, photo of etched grain in reflected light; b3, photo in secondary electrons; (d–e) gold of heterogeneous (fineness variance from 200 to 1120) mosaic structure with signs of initial epigenetic recrystallization, with formation of noncontrasting network of veins of relatively low-fineness gold (dark); (d) (PLK 154) poorly expressed recrystallization; (e) (PLK125) distinctly expressed with formation of larger blocks of different fineness: d1, network of high-grade veinlets and low-grade blocks record initial granulation (recrystallization) stage of gold, photo of etched grain in reflected light; d2–d3, native gold from dolomite–ankerite–quartz metasomatites saturated with submicron fragments of carbonate (dol), arsenopyrite (asp), and micropores, contains small number of isometric and deformed gas bubbles (circled); d2, low-grade veinlets among relatively higher-grade gold; d3, homogeneous gold of average fineness; photo in reflected electrons.(f, g) irregular gold (fineness variance 4000–9500): (e) gold from upper part (oxidation zone) of deposit (PLK103): e1, low- and high-grade intergrown with iron hydroxides, malachite, and native copper, photo in reflected electrons; e2, homogeneous with high-grade boundary intergrown with oxidized arsenopyrite, microbreccia (carbonate (ank) and arsenopyrite (asp) in fine (<1 μm) fragments) and microporous structure, photo in reflected electrons; (g) (PLK117), g1, zonal manifestation of heterogeneity: light, relatively high-grade gold, dark, low-grade, photo of etched grain in reflected light; g2, deformation diffusion boundary on section of tabular (Omchak) gold. Multiple submicron fragments and pores, as well as rare deformed voids (circled). Photo in BSE (a–d) analyst L.O. Magazina, (d–h) analyst E.V. Kovalchuk.

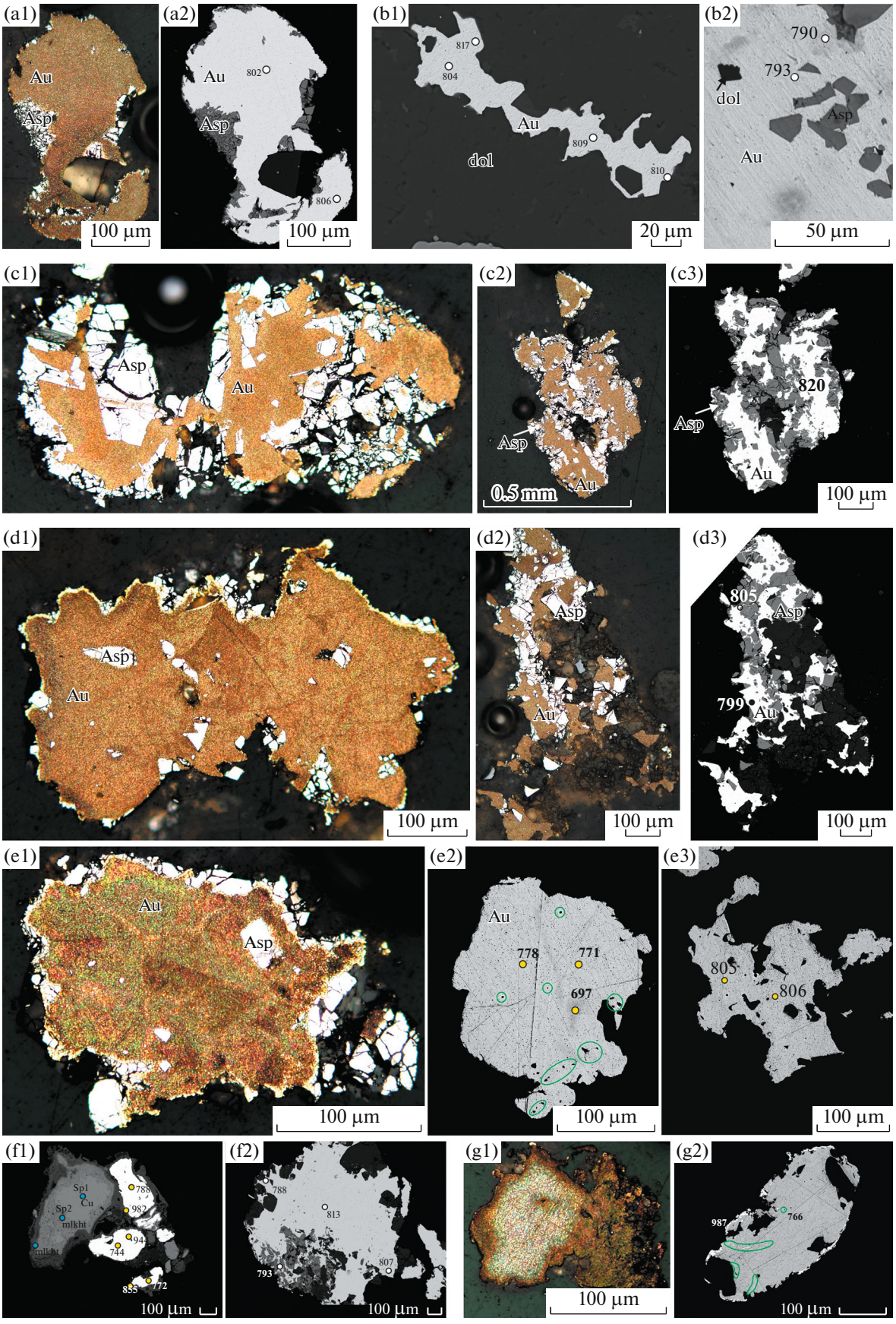
(a1)
Au
Asp
100 μm
(a2)
Au
802
Asp
806
100 μm
(b1)
817
804
Au
809
dol
810
20 μm
(b2)
790
793
dol
Asp
Au
50 μm
(c1)
Asp
Au
(c2)
Asp
Au
0.5 mm
(c3)
820
Asp
Au
100 μm
(d1)
Asp
Au
100 μm
(d2)
Asp
Au
100 μm
(d3)
805
Asp
799
Au
100 μm
(e1)
Au
Asp
100 μm
(e2)
Au
778
771
697
100 μm
(e3)
805
806
100 μm
(f1)
Sp1
Cu
Sp2
mlkht
mlkht
788
982
94
744
855
772
100 μm
(f2)
788
813
793
807
100 μm
(g1)
100 μm
(g2)
987
766
100 μm

K-feldspar or carbonate. Combined inclusions of sericite and chlorite are rare. The compositions of inclusions in native gold does not contradict the hypothesis that native gold crystallized during the formation of synore metasomatites.

In the cross sections of gold grains (Figs. 11h–11j), it can be seen that they contain abundant, evenly distributed impregnation of unidentifiable solid inclusions less than 1 μm in size and voids with the same dimensions. Inhomogeneities and evenly distributed microinclusions were detected only in fine native gold from dolomite–albite metasomatites. Carbonate and arsenopyrite have been identified in native gold from a xenolith of a quartz vein from the Vanin stock (PLK-187), in native gold from the NW flank of ore zone 1 (PLK-108), from boreholes drilled in ore zone 9 (samples PLK-124, 125), and on sections of tabular (Omchak) native gold in the largest acute-angled inclusions (Figs. 11h, 11i). Native gold with a large number of microinclusions is concentrated at the periphery of ore zones, while massive gold is characteristic of the central part of the deposit. Relatively large voids that can be identified as deformed gas bubbles were found in native gold from sample PLK-125 (Fig. 12, d2, d3, g2). Solid-phase acute-angled inclusions in gold can be interpreted as fragments of host metasomatites, and rounded voids (since analysis of the walls of such voids revealed nothing but gold) can be primary syngenetic (according to Lemmlein, 1973) gas or water inclusions.

An indicator of the heterogeneity of native gold is the fineness dispersion, determined by measuring the fineness of individual gold grains in one sample; and is quite consistent with observations on etched gold grains. This indicator varies from 216–155 in samples with homogeneous (monocrystalline?) native gold (PLK124, PLK146, PLK108), up to 200–1120 in samples with significant mottled inhomogeneities (PLK154, PLK125), and reaches 4000–9500 in samples with contrasting inhomogeneities of native gold (PLK103, PLK117). For the deposit as a whole, the index is 2558, which may reflect a large number of analyses to identify heterogeneities or differences in native gold in ore zones 1 and 9 (Table 3).

From the results of etching gold grains and photographing them in reflected light and in backscattered and secondary electrons, it was found that most gold grains have a granular or single-crystal indistinctly zonal structure (Fig. 12). Native gold with a homogeneous composition predominates, while gold grains with high-grade rims or indistinct block structure and irregular silver distribution make up no more than 2–3% of analyzed grains. Native gold with a reduced fineness is found in intergrowths with carbonates and silicates (albite, sericite). In addition, fineness variations result from a decrease in silver content in high-fineness rims that developed around the Omchak gold.

Mottled irregularities are caused by an irregular silver distribution in native gold. The micrographs clearly show a significant number of inhomogeneities associated with redistribution of silver into separate blocks with purification of interblock spaces (Fig. 12, d1, d1). The etched surfaces show signs of initial recrystallization associated with temperature and pressure changes. Observable structures can be compared to structures that form during granulation of quartz.

The BSE photographs of gold grain sections with a general uniform grain density show areas in the form of irregular segregations or zones with increased or decreased reflection of electrons (Fig. 12, b2, d2). For example, in the central part of porous gold (Fig. 12, d2) with a fineness of 763–766, a zone of reduced fineness is observed (680). Quite significant (within 40 units) fineness variations are characteristic of aggregates with spongy-porous (from 783 to 807) and massive native gold (from 795 to 826) (Fig. 11f). These variations may be due to the irregular distribution of silver in the deposition of native gold.

The contrasting heterogeneity in the distribution of areas of different fineness over the grain volume is most clearly expressed in flattened flakelike gold grains with smooth rims (Omchak type) (Fig. 12g). Rims 3–10 μm thick in the marginal parts of gold grains have a fineness from 950 to 998; thin wormlike segregations (10–18 μm along the long side) have the same gold composition, irregularly located in the bulk grain, while the gold fineness varies from 750 to 785. The rims repeat the irregular contours of native gold deposits; their internal boundary is very indistinct.

Invisible Gold

The gold grade in pyrites based on the XRD is low, reaching more that 2σ (30 g/t) in only three out of the 18 measured grains. LA-ICP-MS measurements (60 measurements for 29 grains from 8 samples) showed that in 8% of grains, the content is lower than the sensitivity threshold; in 65% of grains, the content is higher than 1 g/t; and in three grains (5%) of arsenic-bearing pyrite from sample PLK-146, the Au content reaches 213–287 g/t (variance of the sampling, 3076). The gold content in pyrites shows a high correlation with As (+0.77) and significant positive correlation with Sb (0.57) and Pb (0.54). Note the low correlation for the Au–Ag pair (0.34). Transverse profiling across pyrite grains from sample PLK-146 (Figs. 13a, 13b) shows the inhomogeneity of the impurity distribution in pyrite grains associated with both its block structure (shown by the example of Ag) and high fracturing and relict inclusions of host rocks. Depth profiling (Fig. 13c) with a time delay yields similar features of the impurity distribution.

Th gold content in arsenopyrite is 0–70 g/t, exceeding 2σ (34 g/t) in 17.5% of cases (EDX, 40 anal-

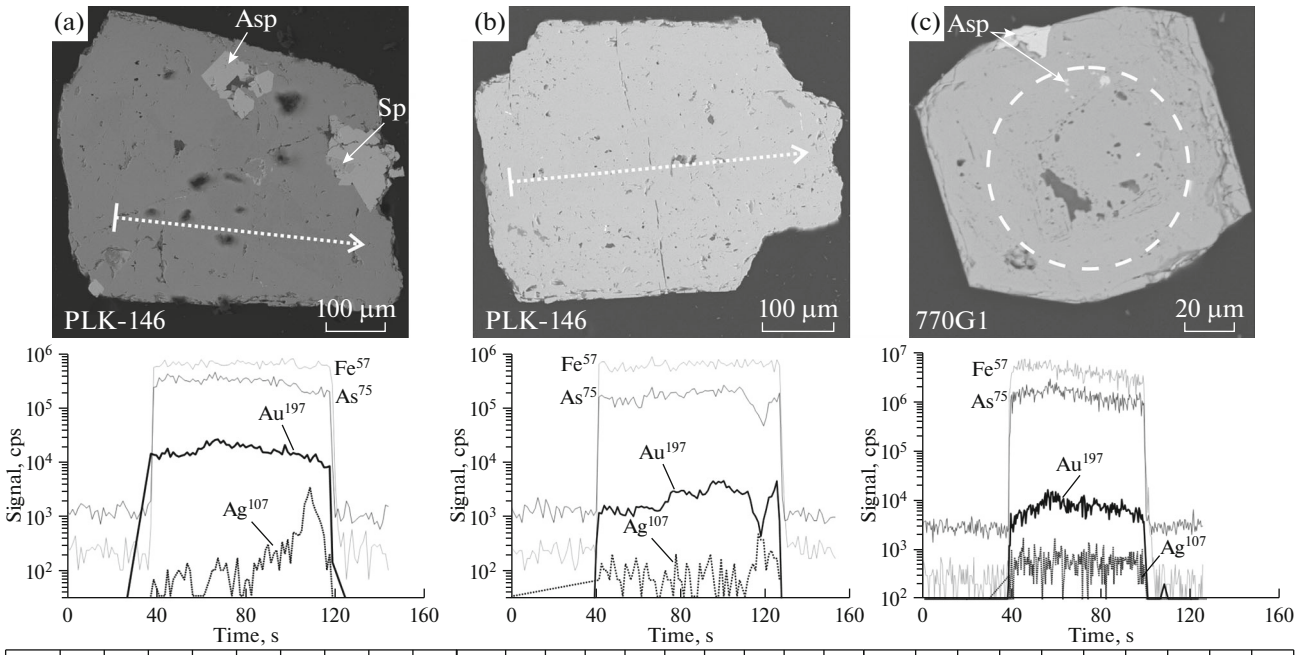

	Au	Ag	Co	Ni	Cu	Zn	Sb	Pb	Bi
Min	213	1.4	0.4	6	139	9	7	137	0.7
Max	287	48	0.6	14	379	742	118	336	4

	Au	Ag	Co	Ni	Cu	Zn	Sb	Pb	Bi
Min	15	2	1	9	23	12	6	15	0.8
Max	57	7	10	81	74	21	26	35	0.9

	Au	Ag	Co	Ni	Cu	Zn	Sb	Pb	Bi
Min	17	1.5	71	411	32	2	24	48	1.7
Max	22	2	94	425	34	3	25	77	2.7

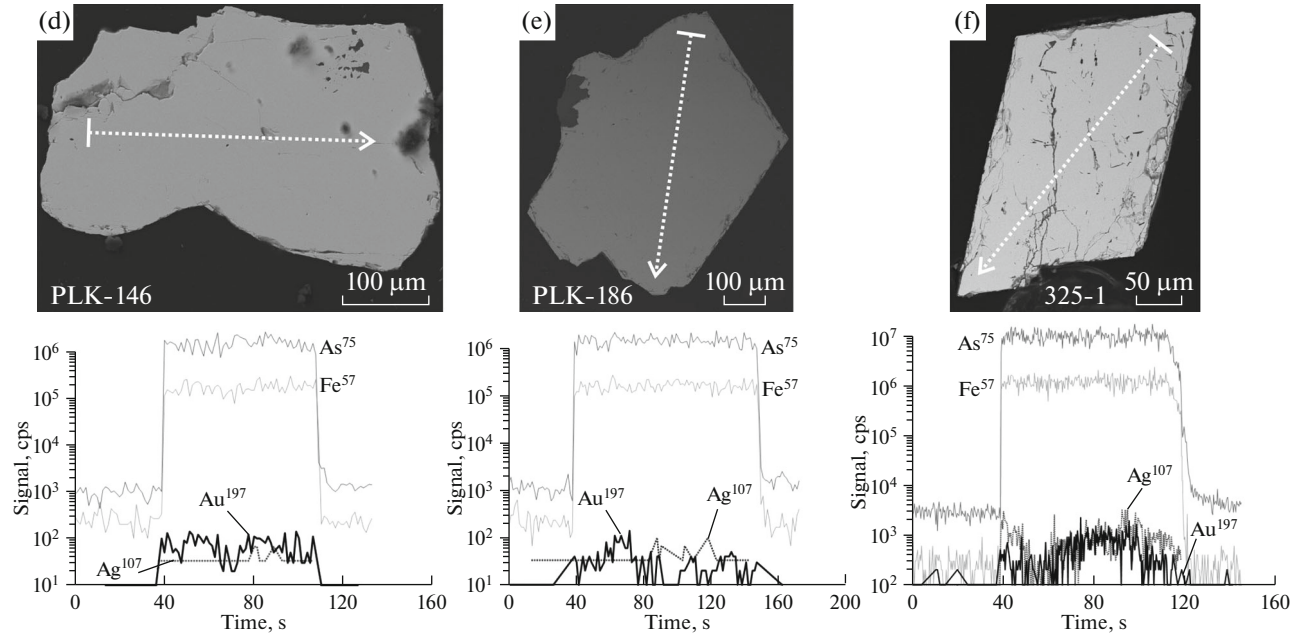

	Au	Ag	Co	Ni	Cu	Sb	Pb	Bi
Min	2	0.4	53	9	6	41	3	–
Max	2	0.6	610	120	8	48	19	1

	Au	Ag	Co	Ni	Cu	Sb	Pb	Bi
Min	0.7	0	3	–	–	29	1.5	–
Max	5.3	2.7	167	29	5	61	9	2

	Au	Ag	Co	Ni	Cu	Zn	Sb	Pb	Bi
Min	0.3	0.5	1.2	–	3.6	37	29.5	3.4	0.3
Max	4.7	7.3	11	2	31	368	142	17	2.4

Fig. 13. Plots of Au and Ag distribution in gold-bearing arsenic-bearing pyrite (a–c) and arsenopyrite (d–f). Vertical axis, number of pulses of corresponding element per second; (signal, cps); horizontal axis, time sweep (time, s); laser beam diameter D = 60 μm; profile length (μm): (1) 400; 2) 426; (3) point analysis, (4) 345; 5) 545; (6) 398; D = 80 μm. Tables show minimum (min) and maximum (max) content of elements (g/t) in profile; dash, below detection limit. Photographs of grains in reflected electrons. Probing profiles obtained by LA-ICP-MS (analyst V.D. Abramova).

yses). Similar results were obtained by laser ablation (LA-ICP-MS, 105 analyses). The gold grade ranges from 0.15 to 7.63 g/t, with grades higher than 1 g/t observed in 47% of samples (variance 1.5). High-level correlations were established for the pairs Sb–Bi (0.71), Co–Ni (0.62), Cr–Zn (0.65), Ag–Pb, Ag–Bi, Pb–Bi, and In–Sn. The gold content showed a positive correlation significance limit with Bi (0.46), Ag (0.39), Sb (0.39), and Pb (0.36). The absence of a relationship between gold microimpurities and Fe, As, and S is confirmed by analysis of the probing profiles of individual arsenopyrite grains from samples with high gold contents—PLK-186 (Fig. 13e) and PLK-146 (Fig. 13d)—and with low gold contents—325-1-7 (Fig. 13f). On both longitudinal and vertical profiles, an extremely uneven distribution of impurities is observed, as well as their localization in individual blocks of arsenopyrite grains.

Among the sulfides of the synore assemblage, only arsenic-bearing pyrite is an invisible gold concentrator. This agrees well with the fact that for some pyrite and native gold, ratios have been established that make it possible to suggest their simultaneous crystallization.

DISCUSSION

The results obtained from studying native gold from the Pavlik deposit can be used to correct ideas about the genesis of gold–quartz objects, to determine the directions of their practical use, including when prospecting for deposits and identifying possible causes of gold losses during ore processing.

Native Gold Size

Our results indicate that the Pavlik deposit is dominated by fine and extremely fine native gold in intergrowths with vein minerals (quartz, carbonates) and sulfides (pyrite, arsenopyrite). In sulfides, both fine native gold in the form of inclusions and native gold included in the crystal lattice of pyrite have been established. Based on the results of microscopic and electron microscopic studies of ores from the Pavlik deposit, we have established finely dispersed (less than 10 μm) and dusty (10–50 μm) native gold. Our sample processing technique used does not allow us to fully assess its relative amount, since the revealed fine native gold, which is found in intergrowths with quartz and carbonates or in the form of the finest isolated impregnations in carbonates, seems inaccessible to gravity extraction with comminution up to 200 mesh (about 74 μm). In order to supplement our understanding of the quantitative ratios of gold of various sizes and the ratio of submicron and associated gold at the deposits of the Omchak ore–placer cluster, we compared our results to those of mining (reports of the Polyus company in 2018–2019 (www.polus.com)), phase analysis (Kazimirov et al., 2008), and technological studies (Sharov et al., 2002) of gold–quartz ores 12 km to the north of the Natalka deposit.

For low-grade ores, gravity–flotation gold recovery at the Natalka deposit ranged from 55.1 to 71.7% according to Polyus reports in 2018–2019, (www.polus.com). Earlier, based on the results of bulk analysis of sulfide monofractions and single grains of arsenopyrite, the opinion was repeatedly expressed (Goncharov et al., 2002; Volkov et al., 2006; Sotskaya, 2017) that the low recovery may be related to a significant amount of gold associated with sulfides at the deposits of the Omchak ore–placer region. The hypotheses about the development of gold bound in sulfides are contradicted by the results of phase analysis of ores (Kazimirov et al., 2008), according to which free (amalgamable) gold in the ores of the Natalka deposit is 82%; gold in intergrowths (cyanided), 4%; in intergrowths with iron hydroxides, 2.5%; in sulfides, 2.3%; in intergrowths with carbonaceous matter, 2.2; and with rock-forming minerals, 7%. The phase analysis data confirm the results of previous technological studies. G.N. Sharov et al. (2002) determined end-to-end gold recovery from gold–quartz ores at 86–87%, and the main losses (12%) are attributed to the stage of obtaining gravity and flotation concentrates (extraction into gravity concentrate, 69.9%; and in flotation (intergrowths with sulfides), 17.8%). After cyanidation of the flotation product, gold is almost completely recovered from sulfides.

Analysis of these data shows that the largest discrepancy (more than 12%) is observed between the amount of free (amalgamated) gold (82%) and the amount of native gold recovered by gravitation (70% or less). This suggests the significant development of finely dispersed gold intergrown with nonfloating quartz, carbonate, and various silicates. Due to its small size, this gold cannot be freed by grinding from intergrowths with nonmetallic minerals and does end up in either gravity or flotation concentrates.

The combined technological scheme developed for the conditions of the Pavlik Gold Mining Company (https://www.arlan.ru/news/685) includes gravity concentration, flotation of gravity tailings, and sorption cyanidation of the obtained gold-bearing sulfide gravity and flotation concentrates. Recovery of gold into a final marketable product, Doré alloy, is 82–83%. Comparing these data with the result of data analysis for the Natalka deposit, we conclude that 17–18% of the weight loss is associated with submicron and dusty native gold. Comparison of these data on losses during development of the Pavlik deposit with the results of grain size distribution analysis (on average, about 6% of gold grains with dimensions less than 100 μm were extracted) makes it possible to increase the estimate of the amount of dusty and submicron native gold (74 μm) to 15–20%.

This confirms our hypotheses about the wide distribution of finely dispersed native gold not bound in

sulfides at the Pavlik deposit and the insignificant development of highly gold-bearing sulfides at the deposits of the Omchak ore–placer cluster, in which gold would have entered the crystal lattice or been in the form of colloid-size impurities, as found at the Nezhdaninskoe, Olympiada, and Sentachan deposits (Genkin et al., 1998).

Possible ways to solve the problem of gold losses can be ultrafine grinding of ores and/or cyanidation of flotation tailings after their treatment with acids for partial elimination of carbonates.

Mineral Deposition Sequence and Changes in the Physicochemical Conditions during Native Gold Deposition

Comparison of our mineral formation sequence data does not contradict the data of predecessors (Tyukova and Voroshin, 2007; Sotskaya, 2017). Metasomatites can be compared with the beresites that formed in tectonite zones of the Nezhdaninskoe (Alpatov, 1998; Bortnikov et al., 2007) and Natalka deposits (Struzhkov et al., 2006; Goryachev et al., 2008). Breccia of host rocks and early quartz with quartz, carbonaceous–quartz, and carbonate–quartz cement has been established in many gold deposits both in the Omchak district (Goncharov et al., 2002) and outside it (Aristov et al., 2016). Such breccia usually mark local extension zones along the strike of strike-slip faults or fault intersection zones. At the Pavlik, in addition to the main ore zone, breccia is often observed in gently dipping veinlets with normal-fault kinematics. The characteristic breccia textures make it possible to relate their formation to hydraulic fracturing phenomena (Konstantinov, 1977; Je'brak, 1997). Pressure variations from 2.5 to 0.5 kbar established by us (Savchuk et al., 2018) at the Pavlik from fluid inclusions in quartz of different ages do not contradict the hypothesis of significant pressure fluctuations during breccia formation. It is possible that high-temperature facies analogs of hydrothermal breccia are the explosive breccia of the Vanin stock described by (Sidorov et al., 2010). The established episodes of quartz–carbonate veinlet formation, as well as the development of hydraulic fracturing-related breccia, allow us to consider that, just like in other orogenic deposits (Sibson et al., 1988), the fluid pressure at the Pavlik deposit repeatedly exceeded the lithostatic pressure. The reason could be seismic events that led to depressurization and development of fracture network in the fault zone.

The relationship between native gold and pyrite does not contradict the hypothesis that native gold at the Pavlik deposit crystallized later than large metasomatic pyrite crystals and at about the same time as pyrite aggregates of one of the late mineral assemblages.

Analysis of the relationships between arsenopyrite and host rocks, metasomatite minerals (albite, potassium feldspar, and carbonates), pyrite, and minerals of the productive (gold-bearing) assemblage suggest that the formation of arsenopyrite, as well as vein, veinlet, and disseminated segregations of pyrite, quartz, ankerite-dolomite, and albite, is a long, continuous, background process. This process can be interrupted by individual tectonic episodes, but it did not stop during the entire period of ore formation at the Pavlik deposit. Note that a change in fluid composition is recorded by the appearance of newly formed potassium feldspar instead of albite in inclusions in native gold and arsenopyrite (Fig. 11i). The simultaneous formation of native gold and some pyrite and/or arsenopyrite (Figs. 6f–6h) does not contradict facts established at other orogenic gold deposits. For example, at the Natalka deposit, arsenopyrites of several generations (Goryachev et al., 2008) formed before, together with, and after native gold. A similar relationship between native gold and arsenopyrite was emphasized by N.V. Petrovskaya for the Sovetskoe deposit (Petrovskaya, 1973, p. 62).

Pyrite and arsenopyrite contain submicroscopic inclusions of native gold and base metal sulfides (Figs. 5g, 6c, 6e–6g, 7a, 7b). Their formation under decreased supersaturation conditions can be explained by a local increase in the concentrations of Au, Zn, Cu, Pb due to adsorption on the growing faces of pyrite and arsenopyrite. It is possible that crystallization of a small amount of sphalerite, chalcopyrite, and galena occurred upon an influx of solutions bearing Zn, Cu, and Pb. Since inclusions are observed quite rarely (one to two grains with inclusions per 10–15 grains without), the second variant seems preferable. In this case, both native gold and base metal sulfides can be deposited at local redox barriers upon partial dissolution of already crystallized pyrite and arsenopyrite (Pokrovski et al., 2002). The closeness of the crystallization time of chalcopyrite, sphalerite, pyrrhotite, and native gold is confirmed by the fact that together they fill cracks in pyrite and arsenopyrite or form intergrowths in quartz–carbonate–sericite aggregates (Figs. 7a, 7b, 7e, 7f). At the same time, veins or halos of dusty gold impregnation are often spatially separated from sulfides (Figs. 7d, 7g, 7h), which can be explained by the low sulfur activity in the gold-bearing fluid, in contrast to fluid bearing As.

Native gold is deposited in rocks in which metamorphic mineral assemblages already exist and regional cleavage has developed (Fig. 5g). The fragmentation of arsenopyrite and the cementing of its fragments with native gold (Figs. 7c, 7g) indicate tectonic events immediately preceding the formation of relatively large native gold segregations. In less brittle quartz–sericite-chlorite–albite–carbonate metasomatic aggregates, the morphology of native gold is subordinate to microcracks that developed along broken grain boundaries. No displacements have been

identified along most cracks containing native gold (e.g., Figs. 7d, 7e). These observations agree well with data from the Bendigo (Wilson et al., 2013) and Fosterville (Voisey et al, 2020) deposits. However, native gold from the Pavlik deposit is confined to detachment and shear fractures and does not show a close relationship with stylolite seams or pressure solution seams, as established at the Fosterville deposit (Voisey et al., 2020). The en echelon cracks filled with native gold in arsenopyrite (e.g., Fig. 7c) may indicate the initial stage of rock failure when the hydrostatic pressure exceeds the lithostatic pressure and brittle deformations develop in the most competent minerals. A local increase in gas-saturated fluid pressure exceeding the ultimate rock strength immediately before native gold deposition may be indicated by the following: parallel formation of veinlike segregations of native gold in brittle sulfides and interstitial growth of native gold in metasomatites; saturation of individual gold grains with micropores and, simultaneously, with fragments of host rocks and minerals of similar size (Figs. 11f–11j, 12, d2, d3, g1).

The levels of invisible gold in arsenopyrite and pyrite from the Pavlik deposit established by point analysis methods are not high, which distinguishes the sulfides of the deposit from sulfides, which were analyzed by A.D. Genkin et al. In the mesothermal gold deposits of Olympiada, Veduga, Nezhdaninskoe, and Sentachan (Genkin et al., 1998). The low contents agree well with the experimental data presented in (Trigub et al., 2017) for pyrite and arsenopyrite crystallization from solutions unsaturated in gold. The gold content is slightly elevated in arsenic pyrite, which is typical of orogenic gold deposits, e.g., Sukhoi Log (Large et al., 2007; Gavrilov and Kryazhev, 2008), Carlin deposits (*Vorontsovskoe* ..., 2016; Cline et al., 2005; Barker et al., 2011), and gold-bearing epithermal objects. As shown in (Reich et al., 2005), the Au/As molar ratio in arsenic-bearing pyrite may be an indicator of the chemical state of Au in pyrite (nanoscale (Au/As > 0.2) or ionic (Au^{1+}) gold), and it also used to determine the saturation state of the solution from which the gold crystallized. The determined levels of gold in arsenic-bearing pyrite from the Pavlik deposit and Au/As < 0.01 (Sidorova et al., 2020) unambiguously indicate that, just like in Carlin deposits, gold in arsenic-bearing pyrite is in the form of a solid solution in the ionic state (Au^{1+}) and undersaturation of the ore-forming fluid in native gold. Thus, analysis of sulfides leads to the conclusion that their crystallization took place from solutions undersaturated in native gold. This hypothesis is contradicted by the fact that, as shown above, most gold at the Pavlik deposit is not bound in sulfides, and finely dispersed gold is at least 15% of the total gold of the deposit by weight. According to data on epithermal deposits (Reich et al., 2005), this may mean that native gold deposition occurs from solutions oversaturated with native gold. The obvious contradiction can be resolved by the hypothesis that the deposition of native gold is an independent process with respect to the formation of sulfides, or that at the time of entry of gold into the ore deposition zone, arsenic-bearing pyrite was absent. Since arsenic-bearing pyrite is a metastable phase that exists over a wide range of pressures and temperatures, the absence of arsenic-bearing pyrite at the time of gold deposition can be considered unlikely. The first hypothesis is more likely. The absence of features of mixing of gold- and sulfur-bearing fluids is explained by the high fluid pressure of the former.

Inhomogeneities of native gold can be used to reveal its gradual growth or recrystallization (*Samorodnoe* ..., 2015). The high homogeneity of native gold at the Pavlik deposit, the absence of growth zones for crystals or twins, poorly developed deformation inhomogeneities in the composition established during etching of gold grains, as well as in the study of gold grains in backscattered electrons, allow us to assume the formation of gold grains with the adhesion of nanosized particles by the self-assembly mechanism (Zhou et al., 2013). This is considered to be the leading mechanism in the formation of native gold at both epithermal (Saunders and Burke, 2017) and orogenic (Voisey et al., 2020) deposits.

The occurence of sorption processes is apparently limited to the effect on the fineness of native gold, which crystallizes in intergrowth with sulfides (>800) and carbonates and silicates (the appearance of small relatively low-fineness grains).

High-fineness rims, as well as initial granulation structures, may be associated with diffusion removal of silver under the influence of later tectonic deformations of gold grains or they record a decrease in the amount of silver in the fluid due to the lower stability of its complex compounds. The latter hypothesis is consistent with a decrease in the fineness of native gold in the lower horizons of the deposit and the fact that the rims are characteristic of gold grains with a certain morphology. According to S.V. Yablokova (Pluteshko et al., 1988), similar heterogeneities in the structure of native gold of the Natalka deposit is explained by the partial diffusion removal of silver under the influence of prolonged heat exposure. This hypothesis is contradicted by the absence of high-grade rims in native gold from a xenolith of a quartz vein in rhyodacites from the Vanin stock (PLK-187).

Relicts of high-grade native gold, as well as structures similar to those of solid solution decomposition, and low-grade zones along the periphery of gold grains of the Natalka deposit allowed predecessors (Pluteshko et al., 1988) to speak about the early stages, accompanied by the deposition of mainly finely dispersed native gold, and late stages of native gold formation. A conclusion on four generations of native gold, the bulk of which formed during two ore deposition stages, was made in (Goncharov et al., 2002). The formation of low-grade native gold crystals, veins of

low-grade native gold in high-grade gold, and deformation and recrystallization of high-grade native gold are associated with Cretaceous rhyolite magmatism (Goryachev et al., 2008). It is assumed that during the late stage, finely dispersed native gold was redeposited and assimilated by large native gold. According to A.D. Genkin et al. (1998), at the Olimpiada, Veduga, Nezhdaninskoe, and Sentachan deposits, chemically bound Au and submicroscopic gold in sulfides (in arsenopyrite and pyrite) was deposited earlier and, apparently, from other fluids (first stage). Native gold in veins or fissures growing on gold-bearing arsenopyrite formed later (second stage). This sequence reflects the evolution of the fluid composition or the involvement of more than one fluid in the ore process. At the same time, there are no features for determining that later native gold formed during the recrystallization of gold-bearing sulfides (Genkin et al., 1998). Coarsening of native gold during recrystallization and redeposition under pressure is considered for the Australian Fosterville deposit (Voisey et al., 2020). At the initial stage, immiscibility of fluids leads to critical supersaturation of fluids and deposition of gold nanoparticles in quartz, along fractures in fault zones. At aseismic moments, in transpressional settings, redistribution and growth of large native gold occurs. In quartz, this process is caused by partial pressure dissolution and removal of matter and accumulation of insoluble gold particles in sutures, and in sulfides, with the development of fracturing and the influence of various electrochemical processes (Voisey et al., 2020).

Our data testify in favor of an independent gold-bearing assemblage, the beginning of the formation of which is accompanied by a change in tectonic setting in the ore deposition zone and the appearance there of ore-forming fluids, with new compositions and physicochemical parameters. Crystallization of most pyrite/arsenopyrite and deposition of most native gold occurs as a result of different processes and from fluids differing in composition and phase state. The morphological features of native gold and, primarily, variations in its size can be explained by the physicomechanical properties of the setting in which it is deposited. The larger the pores and cracks available for deposition of native gold, the larger its segregations. The netlike and mottled nature of native gold inhomogeneities does not contradict the hypothesis of its recrystallization during intraore or subsequent deformation processes, but these phenomena are of limited importance. There are no sufficient grounds to consider native gold deposition at the Pavlik deposit as a process in which the chemical composition of the ore-forming fluid changed significantly. Our data for the Pavlik deposit does not contradict the hypothesis of single-stage deposition of native gold. Similar results indicating the single-stage nature of gold mineralization were obtained by (Ostapenko et al., 2004) for the Degdekan deposit, as well as the Pavlik, located in the Omchak ore–placer cluster.

Prospecting Significance of Features of Native Gold

To determine the prospecting significance of the established morphological and material features of native gold from the Pavlik deposit, we compared these features with those of native gold from other primary and placer deposits of the Omchak ore–placer district (Tables 1, 4).

The morphological features of native gold from the Pavlik deposit and the composition of impurities in it hardly differ from the model features established in (*Samorodnoe* ..., 2015) for native gold from low-sulfide gold–quartz deposits. The main morphological forms of native gold are similar to the forms described by S.V. Yablokova (Pluteshko et al., 1988) at the Natalka deposit. In comparison with the native gold of Natalka, native gold of the Pavlik deposit is characterized by a relatively large size, the absence of crystalline forms of free growth, the presence of spongy–porous gold, and a fineness increased by 20–25‰. It cannot be ruled out that the morphological features of native gold from the Pavlik deposit are associated with the homogeneity of the lithological composition of the host strata (there are no thick sandstone and dike interlayers, and thick vein bodies of early quartz have a limited distribution).

According to the grain size distribution data, the Pavlik deposit is dominated by fracture forms of native gold segregations with close dimensions (0.01–0.5 mm). The size of most native gold in gravity concentrates (0.3 mm) is somewhat larger than that of gold grains (about 0.1 mm with a variation of 0.02–0.4 mm) in gravity concentrates from ores of the Natalka (Pluteshko et al., 1988) and Sukhoi Log deposits (Gavrilov and Kryazhev, 2008).

The composition of the main impurities determined by bulk analysis—Fe, Hg, As, Pb, Bi—is also characteristic of native gold from ores of low-sulfide gold–quartz deposits (*Samorodnoe* ..., 2015). The composition of native gold from the Pavlik deposit is very similar to that of native gold from the Degdekan deposit (Litvinenko, 2009), with the exception of a slightly elevated As content and decreased Pb and Bi contents.

The Pavlik deposit hosts native gold containing voids and monomineralic inclusions of vein and ore mineral fragments. The outer parts of massive homogeneous gold grains may be composed of spongy–porous gold. For ore zone 1, there is a tendency towards an increase in the amount of low-grade gold with depth. There are no distinctly zoned structures or twinned crystals, and deformation and recrystallization structures have been established in single grains. Variations in fineness at the Natalka have been described differently by different authors. S.V. Yablokova (Pluteshko et al., 1988) notes a tendency towards an increase in the amount of high-grade gold with depth; conversely, I.S. Litvinenko (Goncharov et al., 2002) points to an increase in the amount of low-grade gold

Table 4. Summary characteristics of native gold from primary deposits and placers of the Omchak ore–placer cluster

		Pavlik*	Omchak placer (*Placer* ..., 1999; Goncharov et al., 2002)			Natalka (Pluteshko et al., 1988)	Degdekan (Litvinenko, 2009)
			lower part and ruch. Pavlik	top part	placer of Natalkin brook		
Morphology		Interstitial, fissure-veinlet, spongy-porous, tabular (Omchak)	Lumpy scaly spongy lamellar	Lumpy, lamellar, poorly rounded	Spongy-porous, lamellar, dendritic, wire-like	Crystalline, interstitial, fissure-vein	Interstitial, fissure-veinlet, tabular
Internal structure		Homogeneous, granular, micro-inclusions: gas, albite, dolomite, arsenopyrite. High-quality boundaries	High-quality borders. Inclusions of limonite, pyrrhotite, galena	Intergrowths with sulfides, quartz	Iron hydroxides, aggregates with quartz, high-grade edges. Microinclusions of sulfides	Uniform, grainy, low and high quality borders	
Size, mm	Average value	0.3 mm**	0.52 mm**	0.48**	0.34**	0.075 mm***	0.1 mm***
	Dusty and finely dispersed	–0.05 mm from 6 to 26%	Fraction –0.5 mm to 41.6%	Fraction –0.5 mm—up to 52.5%	Fraction –0.5–67.3%	–0.05 mm 2.5–15%	–0.05 mm 16%
	Small	+ 0.1–1 mm more than 88%				+0.1 mm 37–45%	+0.1 mm 54%
	Large		Fraction +2.0 mm – 1.6%	+2.0 mm—6.2%. Nuggets up to 0.3 kg	+2.0 mm—4.8% Nuggets up to 1.13 kg		
Fineness, ‰	Median value	806	N.d.	N.d.	740-797	771	795
	Mean	806 (771)	805	794	776	775	810
	Additional peaks	775–855–985				737–800	755–885–910
Impurities, wt %		Fe(0.3)–Hg(0.15)–As(0.13)–Zn(0.02)–Cu(0.006)–Pb(0.002)	Fe(0.3–5.1)–Cu(0.46)–As(0.1)–Pb(0.1)–Mg(0.1)–Hg(0.08)		Fe–Ca–Mn–Bi–Cu–Co–Sn–Mo–Sb–Pb–As	Pb(0.07)–Fe(0.03)–Zn(0.015)–As(0.005)–Cu(0.004)	Pb(0.81)–Fe(0.6)–Te(0.2)–Hg(0.1)–Sb(0.08)–As(0.04)–Cu(0.005)

* To calculate average fineness of gold, data of 152 EDX analyses and 45 SEM analyses were used;
** by weight;
*** by number of grains. For the Pavlik deposit, the fineness value for the bulk (combined) sample is indicated in brackets.

in the central part of the deposit and at depth. I.S. Litvinenko's observations (Goncharov et al., 2002) do not contradict his data on the concentration of low-grade fine gold in placers in the central part of the Natalka ore field, and high-grade gold in placers on its periphery also agree well with the centrifugal model of placer zoning with respect to probable centers of ore-magmatic systems. (Scriabin, 2010).

The characteristics of the mineral composition of the heavy fraction and features of native gold from placers of streams crossing the ore zones of the Natalka and Pavlik deposits are given according to I.S. Litvinenko's data (Goncharov et al., 2002). These placers are characterized by approximately the same set of heavy fraction minerals (iron hydroxides, pyrite, arsenopyrite, rutile, zircon, anatase, brookite, pyroxene, hornblende, garnet, epidote, spinel, ilmenite), which is determined by the composition of the host rocks and pre- and synore mineral assemblages. The greatest differences are observed in the distribution features of the size and fineness of gold grains. An asymmetric size distribution, with predominance of grades 0.25 and 0.25–0.5 mm with a fineness of about 740–750 is characteristic of native gold from the Natalka Creek placer. This placer hosts nuggets weighing up to 1.2 kg. A symmetric size distribution of native gold with predominance of the class 0.25–0.1 mm with a fineness of about 800 was established for the Pavlik Creek placer.

According to the morphological features of native gold, the Omchak placer is divided into upper and lower parts (*Rossypi* ..., 1999). The upper part of the Omchak placer, the largest reserves of which are located opposite the mouth of Natalks Creek, is characterized by predominance of fine gold. Fractions less than 1 mm constitute about 74.4% by weight. Native gold is intergrown with quartz and sulfides; the average gold fineness is 794. During development, nuggets weighing up to 300 g were often observed. In the lower section, from the mouth of Pavlik Creek, fine and very fine native gold with an average fineness of 805 predominates. The amount of the fraction up to 1 mm reaches 90%. High-grade nuggets are observed on tabular gold grains. Spongy, lumpy forms, flakes, and pebbles are typical. Native gold contains pyrrhotite, limonite, and galena inclusions. Thus, the morphological features of native gold from the placers of the Omchak ore–placer cluster reflect the difference in fineness and grain size distriubtion of native gold from primary sources. The appearance of additional size and fineness peaks is especially significant.

It can be assumed that the identification of native gold in placer halos and placers with similar indicators—moderate fineness, reduced uniform grain size, microporous gold grains, or gold grains with microfragments of albite, sericite, carbonates, arsenopyrite, etc.—will indicate a similar genesis and, accordingly, a significant scale of the primary gold source. The data obtained show that the unimodal distribution of the size and fineness of native gold is not a feature of the scale of ore objects, at least within the Omchak ore–placer cluster.

CONCLUSIONS

Native gold of the Pavlik deposit is found in interstitial and fissure intergrowths with albite, chlorite, sericite, potassium feldspar, carbonates, quartz, and pyrite. The same minerals are found as inclusions in native gold. In arsenopyrite, native gold forms microveins with massive and netlike textures. Arsenopyrite crystals were found growing on the surface of individual gold grains. In some cases, sphalerite and pyrrhotite grains and crystals form induction boundaries with native gold.

The Pavlik deposit is dominated by homogeneous, massive native gold with a size less than 1 mm and average fineness of 806 (from 680 to 990). Finely dispersed (<0.01 mm) gold was found in pyrite, arsenopyrite, and carbonate–quartz intergrowths.

Grain size distribution analysis and study of native gold taken from comminuted samples made it possible to establish mmicroscopic (finely dispersed, dusty, and fine) (peak size at 0.075 mm) and visible (very fine and fine) (peak size at 0.25, 0.55, and 0.85 mm) native gold. The main weight of gold come from gold grains of the fine grade with an average size of 0.3 mm. Comparison of the grain size distribution analysis data with data on the technological properties of ores and results of development of the deposits of the Omchak ore–placer cluster made it possible to establish that the share of dusty and finely dispersed grades accounts for at least 15–20% of the gold weight. Finely dispersed (<0.05 mm) impregnation of native gold in carbonates and host rocks can cause gold losses (up to 18%) during gravity–flotation processing at the Pavlik deposit, as well as at other deposits of the Omchak ore–placer cluster.

The impurities found in bulk analysis of native gold are explained by the presence of various inclusions in it. The amount of impurities detected by local precision methods in native gold is small, and variations in fineness are governed by variations in the amount of silver. The results of studying the composition of native gold indicate the absence of a geochemical relationship with sulfide mineralization.

The mottled structure of inhomogeneities of individual gold grains does not contradict the hypothesis of recrystallization of native gold during postore deformations. In a sharply subordinate amount, gold grains with an irregular distribution of silver, marginal high-grade rims, and internal high-grade microgrooves and individual voids surrounded by high-grade edges were found.

The surface features of gold grains represent a combination of smooth and porous irregular areas with

pitted and porous microsculptures. In a small amount (up to 15%), deposits of native gold were found with a microporous and microbreccia structure with a pore size and inclusions of less than 1 μm. Microscopic native gold and native gold with a large number of microinclusions concentrate at the periphery of ore zones, while coarser-grained and more homogeneous native gold is characteristic of the central part of the deposit.

For the overwhelming majority of pyrite and arsenopyrite, the content of invisible gold does not exceed the limiting contents established in experiments on crystallization of iron sulfides from solutions unsaturated in gold. An elevated invisible gold content >200 g/t was found in three arsenic-bearing pyrite grains out of 60 analyzed.

The relationship of native gold with nonmetallic and ore minerals, the observed morphological features of native gold at the Pavlik deposit, the features of its chemical composition and internal structure do not contradict the hypothesis that gold was deposited during a single mineralization stage during its crystallization in a different substrate: (1) in the intergranular space (quartz–carbonate metasomatites), (2) in the intrafracture space (in arsenopyrite and carbonates), (3) in microcracks in host rocks).

The data obtained do not contradict the hypothesis that the deposition conditions of native gold coincide with only some of the conditions reconstructed from thermobarogeochemical data obtained from sulfide and quartz zone minerals. The generation zones, paths, and conditions for the migration of gold-bearing fluids differ from those in which fluid migration occurs, from which veinlets and veins of the quartz zone are formed, and pyrite and arsenopyrite impregnation of the sulfide zone form.

The generalized comparative description of native gold deposits of the Omchak ore–placer district has prospecting significance (Table 4). The identification of poorly rounded native gold in placers with parameters close to those indicated in Table 4 will make it possible to predict primary mineralization similar in scale and structural localization conditions to large deposits of the Omchak district. The identification of zonally distributed placer halos of native gold with increased and decreased fineness and corresponding size can be used to preliminarily assess the erosion level of primary sources. The reduced grain size and fineness of native gold may indicate that the primary source had eroded. The bimodal character of the size distribution and fineness in one placer, as well as the appearance of nuggets and crystals, can serve as signs of the influence of late magmatism or postore tectonics on the ores of primary sources.

To determine the conditions for the formation of native gold and, accordingly, prospecting signs of gold–quartz objects without additional qualifications, it is possible to use only the typomorphic features of the native gold itself, inclusions in it, and minerals for which simultaneous growth with native gold has been unambigously established. It seems that various inclusions in native gold with a porous surface are promising for identifying sources of gold and reconstructing its crystallization conditions.

ACKNOWLEDGMENTS

The authors are grateful to Magadan geologists V.V. Troitsky and S.M. Lyamin for friendly cooperation and support during our group's entire study at the Pavlik field.

The authors also thank L.O. Magazina, S.E. Borisovsky, E.V. Kovalchuk, V.D. Abramova, S.V. Yablokova, and L.N. Shatilova for the analytical studies.

Lastly, the authors are grateful to the reviewers, whose comments made it possible to supplement and significantly improve the original version of the article.

FUNDING

The study was carried out under program FNI 130: Ore-Forming Processes, Their Evolution in Earth's History, Metallogenic Epochs and Provinces and Their Relationship with the Evolution of the Lithosphere; Mineral Formation Conditions and Distribution Patterns. "Metallogeny of Ore Districts of Volcanoplutonic and Orogenic Fold Belts of the Russian Northeast."

SUPPLEMENTARY INFORMATION

The online version contains supplementary material available at https://doi.org/10.1134/S1075701521010025.

CONFLICT OF INTEREST

The authors declare that they have no conflict of interest.

REFERENCES

Alpatov, V.V., Disseminated gold mineralization of the Nezhdaninskoe deposit, *Otechestvennaya Geol.,* 1998, no. 6, pp. 63–65.

Amosov, R.A. and Vasin, S.L., *Ontogenezis samorodnogo zolota Rossii* (Ontogenesis of Native Gold of Russia) Moscow: TsNIGRI, 1995.

Amuzinskii, V., Anisimova, G., and Zhdanov, Yu., *Samorodnoe zoloto Yakutii. Verkhne-Indigirskii raion* (Native Gold of Yakutia. Upper Indigirka District), Novosibirsk: Nauka, 1992.

Anikeev, N.P., Birkis, A.P., and Drabkin, I.E., *Main tendencies in distribution of gold deposits in the southeastern part of the Main Gold Belt of Northeast USSR, Geneticheskie osobennosti i obshchie zakonomernosti razvitiya zolotoi mineralizatsii Dal'nego Vostoka* (Genetic Features and Common Tendencies in the Evolution of Gold Mineralizaiton of Far East), Moscow, 1966, pp. 152–166.

Aristov, V.V., Spatial regularities of localization of gold ore occurrences in the Yana–Kolyma province, *Russ. Geol. Geophys.,* 2019, vol. 60, no. 8, pp. 879–889.

Aristov, V.V., Babarina, I.I., Grigor'eva, A.V., Alekseev, V.Yu., Prokof'ev, V.Yu., Uzyunkoyan, A.A., Zabolotskaya, O.V., and Titov, S.G., Gold–quartz deposits of the Zhdaninsky ore-placer cluster, Eastern Yakutia: structural control and formation conditions, *Geol. Ore Deposits,* 2016, vol. 59, no. 1, pp. 68–102.

Barker, Sh.L.L., Hickey, K.A., Cline, J.S., Dipple, G.M., Kilburn, M.R., Vaughan, J.R., and Longo, A.A., Uncloaking invisible gold: use of nanoSIMS to evaluate gold, trace elements, and sulfur isotopes in pyrite from Carlin-type gold deposits, *Econ. Geol.,* 2011, no. 7, pp. 897–904.

Bortnikov, N.S., Geochemistry and origin of the ore–forming fluids in hydrothermal–magmatic systems in tectonically active zones, *Geol. Ore Deposits,* 2006, vol. 48, no. 1, pp. 1–22.

Bortnikov, N.S., Bryzgalov, I.A., Krivitskaya, I.I., Prokof'ev, V.Yu., and Vikent'eva, O.V., The Maiskoe multimegastage disseminated gold–sulfide deposit (Chukotka, Russia): mineralogy, fluid inclusions, stable isotopes (O and S), history, and conditions of formation, *Geol. Ore Deposits,* 2004, vol. 46, no. 6, pp. 409–440.

Bortnikov, N.S., Gamyanin, G.N., Alpatov, V.V. Nosik, L.P., Naumov, V.B., and Mironova, O.F., Mineralogy, geochemistry and origin of the Nezhdaninsk gold deposit (Sakha-Yakutia, Russia), *Geol. Ore Deposits,* 1998, vol. 40, no. 2, pp. 121–138.

Bortnikov, N.S., Gamyanin, G.N., Vikent'eva, O.V., Prokof'ev, V.Yu., Alpatov, V.A., and Bakharev, A.G., Fluid composition and origin in the hydrothermal system of the Nezhdaninsky Gold Deposit, Sakha (Yakutia), Russia, *Geol. Ore Deposits,* 2007, vol. 49, no. 2, pp. 87–128.

Boyle, R.W., The Geochemistry of Gold and its Deposits, *Can. Geol. Surv. Bull.,* 1979, no. 280.

Buryak, V.A., Mikhailov, B.K., and Tsymbalyuk, N.V., Genesis, distribution, and prospects of gold and PGE potential of black shales, *Rudy Met.,* 2002, no. 6, pp. 25–36.

Chernyshev, I.V., Bortnikov, N.S., Chugaev, A.V., Gamyanin, G.N., and Bakharev, A.G., Metal sources of the large Nezhdaninsky orogenic gold deposit, Yakutia, Russia: results of high-precision MC-ICP-MS analysis of lead isotopic composition supplemented by data on strontium isotopes, *Geol. Ore Deposits,* 2011, vol. 52, no. 5, pp. 353–373.

Chugaev, A.V., Chernyshev, I.V., Gamyanin, G.N., Bortnikov, N.S., and Baranova, A.N., Rb–Sr isotopic systematic of hydrothermal minerals, age, and matter sources of the Nezhdaninskoe Gold Deposit (Yakutia), *Dokl. Earth Sci.,* 2010, vol. 434, no. 4, pp. 1337–1341.

Cline, J.S., Hofstra, A.H., Muntean, J.L., Tosdal, R.M., and Hickey, K.A., Carlin-type gold deposits in Nevada: critical geologic characteristics and viable models, Hedenquist, J.W, Thompson, J.F.H., Goldfarb, R.J., Richards, J.P., Eds., *Econ. Geol.,* 2005, 100th Anniversary Volume, pp. 451–454.

Cox, S.F., Coupling between deformation, fluid pressures and fluid flow in ore-producing hydrothermal systems at depth in the crust, *Econ. Geol.,* 2005, vol. 100, pp. 39–75.

Eremin, R.A., Voroshin, S.V., Sidorov, V.A., Shakhtyrov, V.G., Pristavko, V.A., and Gashtold, V.V., Geology and genesis of the Natalka gold deposit, northeast Russia, *Int. Geol. Rev.,* 1994, pp. 1113–1138.

Firsov, L.V., *Zoloto–kvartsevaya formatsiya Yano–Kolymskogo poyasa* (Gold–Quartz Formation of the Yana–Kolyma Belt), Novosibirsk: Nauka, 1985.

Gamyanin, G.N., *Mineralogo–geokhimicheskie aspekty zolotogo orudeneniya Verkhoyano–Kolymskikh mezozoid* (Mineralogical–Geochemical Aspects of Gold Mineralization of the Upper Yana–Kolyma Mesozoides), Moscow: GEOS, 2001.

Gavrilov, A.M. and Kryazhev, S.G., Mineralogical–geochemical features of ores of the Sukhoi Log deposits, *Razved. Okhr. Nedr,* 2008, no. 8, pp. 3–16.

Gel'man, M.L., Role of regional metamorphism in gold mineralization of Northeast USSR, *Dokl. Akad. Nauk SSSR,* 1976, vol. 230, no. 6, pp. 1406–1409.

Genkin, A.D., Bortnikov, N.S., Safonov, Y.G., Kerzin, A.L., Cabri, L.J., Mcmahon, G., Wagner, F.E., Friedl, J., Stanley, C.J., and Gamyanin, G.N., A multidisciplinary study of invisible gold in arsenopyrite from four mesothermal gold deposits in Siberia, Russian Federation, *Econ. Geol.,* 1998, vol. 93, pp. 463–487.

Goldfarb, R.J., Baker, T., Dube, B., Groves, D.I., Hart, C.J.R., and Gosselin, P., Distribution, character, and genesis of gold deposits in metamorphic terranes, *Econ. Geol.,* 2005, 100th Anniversary volume, pp. 407–450.

Goldfarb, R.J., Groves, D.I., and Gardoll, S., Orogenic gold and geologic time: a synthesis, *Ore Geol. Rev.,* 2001, pp. 1–75.

Goldfarb, R.J., Taylor, R.D., Collins, G.S., Goryachev, N.A., and Orlandini, O.F., Phanerozoic continental growth and gold metallogeny of Asia, *Gondwana Res.,* 2014, no. 25, pp. 48–102.

Goldfarb, R.J. and Groves, D.I., Orogenic gold: common or evolving fluid and metal sources through time, *Lithos,* 2015, pp. 2–26.

Goncharov, V.I., Voroshin, C.B., and Sidorov, V.A. *Natalkinskoe zolotorudnoe mestorozhdenie* (Natalka Gold Deposit), Magadan: SVKNII DVO RAN, 2002.

Goryachev, N.A., Noble metal ore genesis and mantle–crust interaction, *Russ. Geol. Geophys.,* 2014, vol. 55, no. 2, pp. 252–258.

Goryachev, N.A., *Geologiya mezozoiskikh zoloto–kvartsevykh poyasov Severo–Vostoka Azii* (Geology of Mesozoic Gold–Quartz Belts of Northeast Asia), Magadan, 1998.

Goryachev, N.A., Vikent'eva, O.V., Bortnikov, N.S., Prokof'ev, V.Yu., Alpatov, V.A., and Golub, V.V., The world-class Natalka Gold Deposit, Northeast Russia: REE patterns, fluid inclusions, stable oxygen isotopes, and formation conditions of ore, *Geol. Ore Deposits,* 2008, vol. 50, no. 5, pp. 362–390.

Groves, D.I., *The crustal continuum model for Late Archaean lode-gold deposits of the Yilgarn Block*, Western Australia, *Miner. Deposita,* 1993, pp. 366–374.

Groves, D.I., Goldfarb, R.J., Robert, F., and Hart, C.J.R., Gold deposits in metamorphic belts: overview of current understanding, outstanding problems, future research, and exploration significance, *Econ. Geol.,* 2003, vol. 98, pp. 1–29.

Je'brak, M., Hydrothermal breccias in vein type ore deposits: a review of mechanisms, morphology and size distribution, *Ore Geol. Rev.,* 1997, no. 12, pp. 111–134.

Kazimirov, M.P, Nikitenko, E.M., Lukinykh, V.E., and Novikova, T.M., Application of technological methods of

sample preparation for assessment of reserves of large-volume gold deposits by the example of the Natalka deposit, *Zolotodobycha,* 2008, no. 119. https://zolotodb.ru/article/11171

Kerrich, R., Mesothermal gold deposits: a critique of genetic hypotheses, *Greenstone Gold and Crustal Evolution: Geological Association of Canada. NUNA Conference,* Robert, F., Sheahan, P.A., and Green, S.B., Eds., 1991, pp. 13–31.

Konstantinov, M.M., Genetic types of ore-bearing breccias, *Sov. Geol.,* 1977, no. 3, pp.124–128.

Konstantinov, M.M., Ore formation systems in the Earth's crust, *Izv. Vyssh. Ucheb. Zaved., Geol. Razved.,* 2009, no. 5, pp. 22–28.

Konstantinov, M.M., Nekrasov, E.M., Sidorov, A.A., and Struzhkov, S.F., *Zolotorudnye giganty Rossii i mira* (Gold Giants of Russia and World), Moscow: Nauchnyi mir, 2000.

Konstantinovskii, A.A., Sedimentary formations of the Verkhoyansk Belt and settings of their accumulation, *Lithol. Miner. Resour.,* 2009, vol. 40, no. 1, pp. 65–86.

Koval'chuk, E.V., Tagirov, B.R., Filimonova, O.N., Nikol'skii, M.S., and Chareev, D.A., Range of concentrations and speciation of "invisible" Ar in synthetic arsenopyrite, *Osnovnye problemy v uchenii ob endogennykh rudnykh mestorozhdeniyakh: novye gorizonty. Mater. Vseross. konf., posvyashch. 120–letiyu so dnya rozhdeniya vydayushchegosya rossiiskogo uchenogo akademika A.G. Betekhtina* (Main Problems in the Concept of Endogenous Ore Deposits: New Horizons. Proc. All-Russian Conference on the 120th Anniversary of Eminent Russian Scientist, Academician A.G. Betekhtin), Moscow: IGEM, 2017, pp. 204–207.

Kryazhev, S.G., Genetic Models and Criteria for Prediction of Gold Deposits in the Carbonaceous–Terrigenous Complexes, *Doctoral (Geol.–Min.) Dissertation,* Moscow: TsNIGRI, 2017.

Large, R.R., Maslennikov, V.V., Robert, F., Danyushevsky, L.V., and Chang, Z., Multistage sedimentary and metamorphic origin of pyrite and gold in the giant Sukhoi Log deposit, Lena gold province, Russia, *Econ. Geol.,* 2007, vol. 102, no. 7, pp. 1233–1267.

Lemmlein, G.G., *Morfologiya i genezis kristallov* (Morphology and Genesis of Crystals), Moscow: Nauka, 1973.

Litvinenko, I.S., The conditions of existence and typomorphism of native gold in ores of the Degdekanskoe deposit (northeastern Russia) in black shale strata, *Russ. Geol. Geophys.,* 2009, vol. 50, no. 6, pp. 691–697.

Metallogenesis and Tectonics of the Russian Far East, Alaska, and the Canadian Cordillera. Nokleberg, W.J., Bundzen, T.K., Eremin, R.A., and Ratkin, V.V., Eds., *U.S. Geol. Surv. Prof. Pap.,* 2005, no. 1697.

Mikhailov, B.K., Struzhkov, S.F., Aristov, V.V., Natalenko, M.V., Tsymbalyuk, N.V., Tyamisov, N.E., and Uzyunkoyan, A.A., Gold potential of the Yana–Kolyma province, *Rudy Met.,* 2007, no. 5, pp. 4–17.

Moskvitin, S.G., Anisimova, G.S., Zhdanov, Yu.Ya., Amuzinskii, V.A., Balandin, V.A., Kopylov, P.A., and Skryabin, A.I., *Samorodnoe zoloto Yakutii (Kularskii raion)* (Native Gold of Yakutia. Kular District), Novosibirsk, Nauka, 1997.

Nesbitt, B.E., *Phanerozoic gold deposits in tectonically active continental margins, Gold Metallogeny and Exploration,* Glasgow and London: Blackie and Son Ltd, 1991.

Nikolaeva, L.A., Nekrasova, A.N., Milyaev, S.A., Yablokova, S.V., and Gavrilov, A.M., Geochemistry of native gold from deposits of various types, *Geology of Ore Deposits,* 2013, vol. 55, p. 176–184.

Novgorodova, M.I., Agakhanov, A.A., Dikaya, T.V., Gamyanin, G.N., and Zhdanov, Yu.Ya., Microspherules of native gold, sulfides, and sulfosalts in gold ores, *Geochem. Int.,* 2004, vol.42, no. 2, pp. 122–133.

Ostapenko, L.A., Struzhkov, S.F., Ryzhov, O.B., Tsymbalyuk, N.V., and Evtushenko, M.B., Assessment of reliability of ore sampling for large-volume gold deposits in the terrigenous sequences by the example of the Degdekan deposit, *Rudy Met.,* 2004, no. 2, pp. 42–55.

Palymskii, B.F., Goryachev, N.A., Akinin, V.V., Golubenko, I.S., and Lyamin, S.M., Late Mesozoic plutonic series of the Okhotsk–Kolyma region, *Vestn. SVNTs DVO RAN,* 2015, no. 2, pp. 3–14.

Petrovskaya, N.V., *Samorodnoe zoloto* (Native Gold), Moscow: Nauka, 1973.

Phillips, G.N., Australian and global setting for gold in 2013, *Proc. World Gold 2013,* Brisbane, 2013, pp. 15–22.

Plotinskaya, O.Yu. and Abramova, V.D., Zoning of pyrite of copper-porphyry deposits of the South Urals as reflection of the evolution of the porphyry–epithermal system: PCMA and LA–ICP–MS), *Osnovnye problemy v uchenii ob endogennykh rudnykh mestorozhdeniyakh: novye gorizonty. Mater. Vseross. konf., posvyashch. 120–letiyu so dnya rozhdeniya vydayushchegosya rossiiskogo uchenogo akademika A.G. Betekhtina* (Main Problems in the Theory of Endogenous Ore Deposits: New Horizons. Proc. All-Russ. Conf. on 120th of Eminent Russian Scientist, Academician A.G. Betekhtin), Moscow: IGEM RAN, 2017, pp. 315–318.

Pluteshko, V.P., Yablokova S.V., and Yanovskii V.M., Natalka deposit, *Geologiya zolotorudnykh mestorozhdenii Vostoka SSSR* (Geology of Gold Deposits of East USSR), Moscow: TsNIGRI, 1988, pp. 126–140.

Pokrovski, G.S., Kara, S., and Roux, J., Stability and solubility of arsenopyrite, FeAsS, in crustal fluids, *Geochim. Cosmochim. Acta,* 2002, vol. 6, no. 13, pp. 2361–2378.

Politov, V.K., Struzhkov, S.F., Natalenko, M.V., and Golubev, S.Yu., Main features of the geology and gold metallogeny of the Central-Kolyma district, *Rudy Met.,* 2008, no. 4, pp. 16–30.

Prokofiev, V.Y., Banks, D.A., Lobanov, K.V., et al., Exceptional concentrations of gold nanoparticles in 1.7 Ga fluid inclusions from the Kola Superdeep Borehole, Northwest Russia, *Sci Rep.,* vol. 10, 1108 (2020). https://doi.org/10.1038/s41598-020-58020-8

Prostranstvennye metallogenicheskie taksony. Seriya "Modeli mestorozhdenii almazov, blagorodnykh i tsvetnykh metallov" (Spatial Metallogenic Taxons. Series Models of Deposits of Diamond, Noble and Non–Ferrous Metals), Krivtsov, A.I., Ruchkin, G.V., Eds., Moscow: TsNIGRI, 2002.

Reich, M., Kesler, S.E., Utsunomiya, S., Palenik, C.S., Chryssoulis, S.L., and Ewing, R.C., Solubility of gold in arsenian pyrite, *Geochim. Cosmochim. Acta,* 2005, vol. 69, no. 11, pp. 2781–2796.

Rossypi zolota Severo-Vostoka Rossii (modeli dlya prognoza, poiskov i razvedki) (Gold Placers of Northeast Russia: Models for Prediction, Survey, and Prospecting), Konstantinov, M.M., Zinnatullin, M.Z., Pruss, Yu.V., Eds., Moscow: KPR on Magadan district, MPR RF, 1999.

Safonov, Yu.G., Topical issues of the theory of gold deposit formation, *Geol. Ore Deposits,* 2010, vol. 52, no. 6, pp. 438–458.

Samorodnoe zoloto rudnykh i rossypnykh mestorozhdenii Rossii: atlas (Native Gold of Northeast Russia: Models for Prediction and Prospecting), Nikolaeva, L.A., Gavrilov, A., Nekrasova, A.N., Yablokova, C.B., and Shatilova, L.V., Moscow: Akvarel', 2015.

Saunders, J. and Burke, M., Formation and aggregation of gold (electrum) nanoparticles in epithermal ores, *Minerals,* 2017, vol. 7, no. 9, pp. 163–174.

Savchuk, Yu.S., Volkov, A.V., Aristov, V.V., Sidorov, V.A., and Lyamin, S.M., Structure and composition of gold lodes of the Pavlik deposit, *Rudy Met.,* 2018, no. 2, pp. 77–85.

Savva, N.E. and Preis, V.K., *Atlas samorodnogo zolota Severo-Vostoka SSSR* (Atlas of Native Gold of Northeast USSR), Moscow: Nauka, 1990.

Shakhtyrov, V.G., *Ten'kinskii deep-seated fault: tectonic position, infrastructure, and ore potential, Geologicheskoe stroenie, magmatizm i poleznye iskopaemye Severo-Vostochnoi Azii* (Geological Structure, Magmatism, and Mineral Resources of Northeast Asia), Magadan: SVKNII DVO RAN, 1997, pp. 62–64.

Sharov, G.N., Bashlykova, T.V., Pakhomova, G.A., *Tekhnologii izvlecheniya blagorodnykh metallov iz rud mestorozhdenii osnovnykh geologo-promyshlennykh tipov. Atlas. Kniga 2* (Technology of Extraction of Noble Metals from Ores of the Deposits of the Main Geological–Economic Types. Atlas. Book 2), Moscow–Kemerovo, 2002.

Shilo, N.A., *Uchenie o rossypyakh* (The Theory of Placers), Moscow: Izd-vo Akademii gornykh nauk, 2000.

Sibson, R.H., Robert, F., and Poulsen, K.H., High-angle reverse faults, fluid-pressure cycling, and mesothermal gold–quartz deposits, *Geology,* 1988, vol. 16, pp. 551–555.

Sidorov, A.A., Sidorov, V.A., and Volkov, A.V., Gold-bearing explosive breccias of the Vanin Stock: a new type of mineralization in northeastern Russia, *Dokl. Earth Sci.,* 2010, vol. 435, no. 6, pp. 1596–1601.

Sidorov, A.A. and Tomson, I.N., Conditions of formation of sulfidized black shales and their metallogenic significance, *Tikhookean. Geol.,* 2000, vol. 19, no. 1, pp. 37–49.

Sidorova, N.V., Aristov, V.V., Grigor'eva, A.V., and Sidorov, A.A., "Invisible" gold in pyrite and arsenopyrite of the Pavlik deposit (northeast Russia), *Dokl. Earth Sci.,* 2020, vol. 495, no.1, pp. 25–30.

Skornyakov, P.I., Systematics of gold deposits of NE USSR, *Mater. Geol. SV SSSR,* 1949, no. 4, pp. 52–62.

Skryabin, A. I., *Rekonstruktsiya lateral'noi zonal'nosti zolotogo orudeneniya (Yano–Kolymskii poyas)* (Reconstruction of Lateral Zoning of Gold Mineralization: Yana–Kolyma Belt), Yakutsk: Sib. Otd. RAN, 2010.

Sotskaya, O.T., Mineralogical and Geochemical Features of Gold–Sulfide-Disseminated Deposits in the Southern Yana–Kolyma Gold Belt, *Extended Abstract of Candidate's (Geol.–Min.) Dissertation,* Magadan, 2017.

Struzhkov, S.F., Natalenko, M.V., Chekvaidze, V.B., Isakovich, I.Z., Golubev, S.Yu., Danil'chenko, V.A., Obushkov, A.V., Zaitseva, M.A., and Kryazhev, S.G., Multifactor model of the Natalka gold deposit, *Rudy Met.,* 2006, no. 3, pp. 34–44.

Tektonika, geodinamika i metallogeniya territorii Respubliki Sakha (Yakutiya) (Tectonics, Geodynamics, and Metallogeny of Sakha Republic (Yakutia), Moscow: MAIK "Nauka. Interperiodika", 2001.

Tomkins, A.G. and Grundy, C., Upper temperature limits of orogenic gold deposit formation: constraints from the granulite–hosted Griffin's Find deposit, Yilgarn Craton, *Econ. Geol.,* 2009, vol. 104, pp. 669–685.

Trigub, A.L., Tagirov, B.R., Kvashnina, K.O., Chareev, D.A., Nickolsky, M.S., Shiryaev, A.A., Baranova, N.N., Kovalchuk, E.V., and Mokhov, A.V., X-ray spectroscopy study of the chemical state of "invisible" Au in synthetic minerals in the Fe–As–S system, *Am. Mineral.,* 2017, pp. 1057–1065.

Tyukova, E.E. and Voroshin, S.V., *Sostav i paragenezisy arsenopirita v mestorozhdeniyakh i vmeshchayushchikh porodakh Verkhnekolymskogo regiona (k interpretatsii genezisa sul'fidnykh assotsiatsii)* (Composition and Paragenesis of Arsenopyrite in the Deposits and Host Rocks of the Upper Kolkyma District: Interpretation of Genesis of Sulfide Associations), Magadan, SVKNII DVO RAN, 2007.

Vikent'eva, O.V., Bortnikov, N.S., Vikentyev, I.V., Groznova, E.O., Lyubimtseva, N.G., and Murzin, V.V., The Berezovsk giant intrusion-related gold–quartz deposit, Urals, Russia: evidence for multiple magmatic and metamorphic fluid reservoirs, *Ore Geol. Rev.,* 2017, vol. 91, pp. 837–863.

Voisey, C.R., Willis, D., Tomkins, A.G., Wilson, C.J.L., Micklethwaite, S., Salvemin, F., Bougoure, J., and Rickard, W.D.A., Aseismic refinement of orogenic gold systems, *Econ. Geol.,* 2020, vol. 115, no. 1, pp. 33–50.

Volkov, A.V., Genkin, A.D., and Goncharov, V.I., Gold speciation in the ores of the Natalka and Maiskoe deposits, *Tikhookean. Geol.,* 2006, vol. 25, no. 6, pp. 18–29.

Vorontsovskoe zolotorudnoe mestorozhdenie. Geologiya, formy zolota, genezis (Vorontsovskoe Gold Deposit. Geology, Gold Speciation, and Genesis), Vikentyev, I.V., Tyukova, E.E., Murzin, V.V., Vikent'eva, O.V., and Pavlov, L.G., Eds., Yekaterinburg: Fort Dialog–Iset', 2016.

Voroshin, S.V., Tyukova, E.E., Newberry, R.J., and Layer, P.W., Orogenic gold and rare metal deposits of the Upper Kolyma district, northeastern Russia: relation to igneous rocks, timing, and metal assemblages, *Ore Geol. Rev.,* 2014, vol. 62, pp. 1–24.

Wilson, C.J.M., Schaubs, P.M., and Leader, L.D., Mineral precipitation in the quartz reefs of the Bendigo gold deposit, Victoria, Australia, *Econ. Geol.,* 2013, vol. 108, pp. 259–278.

www.arlan.ru/news/685/

www.nedradv.ru

www.polyus.com

www.arlan.ru

Zhou, Q., Wang, B., Wang, P., Dellago, C., Wang, Y., and Fang, Y., Nanoparticle-based crystal growth via multistep self–assembly, *CrystEng–Comm.,* 2013, vol. 15, pp. 5114–5118.